C.P. No. 208
(15,120)
A R C. Technical Report

C.P. No. 208
(15,120)
A R C. Technical Report

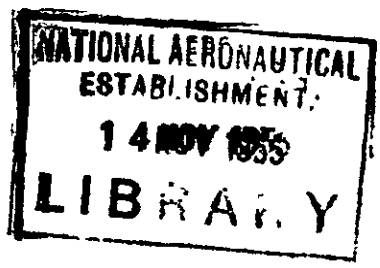

MINISTRY OF SUPPLY

AERONAUTICAL RESEARCH COUNCIL

CURRENT PAPERS

Theory of the Broad-Bladed Propeller

By

G. I. Ginzel

LONDON . HER MAJESTY'S STATIONERY OFFICE

1955

SIX SHILLINGS NET

C.P. No. 208

ADMIRALTY RESEARCH LABORATORY

A.R.L./R3/G/HY/7/1

Theory of the Broad-Bladed Propeller

- By -
G. I. Ginzel

June, 1952

Abstract

The standard propeller theory is that of the lifting line and therefore strictly valid for narrow blades only. The present first step towards a theory of the propeller blade as a lifting surface considers besides the downwash which induces an inclination of flow, the downwash derivative and the corresponding induced camber of the streamlines in the special case of shock free entry of flow at the leading edge. The result is given in the form of a correction factor to be applied to the camber ratio of the section derived by the lifting line theory. The first part (sections 1 to 9) of the present paper presents again the theory of Ludweig and Ginzel[1] but with a modified mathematical derivation.

In the second part the influence on the camber correction factor of blade shape, of number of blades and of circulation distribution over the radius is shown. The condition of uniform minimum pressure over the radius determines an adequate shape of the blade which depends on the circulation distribution. Unfortunately the section camber ratio tends to infinity at the tip for these adequate blade shapes in particular for the so-called best distribution (with the usual blade shapes). Therefore a modified circulation distribution but retaining the previous blade shape is suggested and this case of constant downwash derivative over the radius proves to be of special interest.

Contents/

Contents

---

1. Introduction

In high-speed flight the lift coefficient of the modern aerofoil is small. The aim is a drag coefficient as low as possible. For this purpose so-called laminar profiles have been developed. These profiles show for certain low lift coefficients a more or less constant pressure distribution over the chord and by this means the flow remains laminar over a large range of Reynolds numbers and the drag is accordingly low.

Ship propellers running at a high number of revolutions and producing a high forward speed are in the danger of cavitating. To avoid surface cavitation the pressure should be distributed as uniformly as possible over the surface. Suction peaks must be avoided and the pressure distribution over the chord should be approximately constant. Therefore both in aerofoil and in propeller theory shock free entry of flow at the leading edge plays an important part. It has been suggested

that/

that laminar profiles should be used also for ship propellers and for turbine blades. Since for these profiles low drag is guaranteed only for a very small range of angles of incidence their application for propellers is rather doubtful because the accuracy of propeller theory is not so good as the accuracy of aerofoil theory. In particular the usual propeller theory of the lifting line must be corrected before such refinements as laminar profiles can be introduced.

Certainly the presuppositions of the theory of the lifting line do not hold for the broad blade of the modern ship propeller. These presuppositions are high aspect ratio that is small ratio of chord over span or chord over radius respectively so that the conditions in a section perpendicular to the radius are nearly those of two dimensional flow. With small chord ratios the variation of the downwash velocity along the chord may be neglected, the induced angle of incidence depends on the radius only and the formulae of two-dimensional flow can be used by introducing an effective angle of incidence (geometrical angle of incidence reduced by the induced angle of incidence).

With large chord ratios the variation of the downwash velocity along the chord cannot be neglected. In first approximation this variation is given by the downwash derivative and defines the curvature of the streamlines. In curved flow the camber ratio of the profile is less effective than in straight flow, therefore the effective camber ratio is the geometrical camber ratio reduced by the induced camber ratio. The aim of the following investigation is to determine the effective camber ratio for circular arc camber line aerofoils and propellers in a flow meeting the leading edge with shock free entry. Then the flow is symmetrical to the midpoint of the chord and the camber ratio of the flow must be calculated at this point. All aerofoil or propeller theories are based on the condition that the flow has to follow the surface of the profile. Prandtl's theory of the lifting line introduces the correct direction of flow

$$\alpha_{geom} = \alpha_{eff} + \alpha_i \qquad \ldots(1)$$

where α is the angle of incidence and the suffices mean geometrical, effective and induced respectively. The new theory ensures that both the direction and the camber of flow are correct, so besides (1) another equation (2) has to be fulfilled

$$\frac{f_{geom}}{c} = \frac{f_{eff}}{c} + \frac{f_i}{c} \qquad \ldots(2)$$

where f is the camber and c the chord of the profile.

2. The Lifting Surface at the Condition of Shock Free Entry

The tangent of the streamline element ds relative to the inflow is the ratio of the downwash velocity w_d and the inflow velocity V

$$\tan \alpha = \frac{w_d}{V} \qquad \ldots(3)$$

Hence/

Hence the radius R_o of its curvature is given by

$$\frac{1}{R_o} = \frac{1}{V} \frac{\frac{dw_d}{ds}}{\sqrt{1 + \left(\frac{w_d}{V}\right)^2}^3}$$

or with small w_d/V .

$$\frac{1}{R_o} = \frac{1}{V} \frac{dw_d}{ds} \qquad \ldots(4)$$

instead of using the radius of curvature the camber ratio $\frac{f}{c}$ can be introduced in accordance with Figure 1

$$\left(\frac{c}{2}\right)^2 = f\,(2R_o - f)$$

or for small $\left(\frac{f}{c}\right)^2$

$$\frac{f}{c} = \frac{1}{8} \frac{c}{R_o} = \frac{c}{8V} \frac{dw_d}{ds} \qquad \ldots(5)$$

The camber ratio of the streamline with chord c is from (5) given by the downstream derivative at the midpoint of the chord produced by both the lifting vortices and the trailing vortices of the whole system. According to (2) the expression (5) determines the geometrical camber of the profile

$$\frac{f_{geom}}{c} = \frac{c}{8V} \frac{dw_d}{ds} \qquad \ldots(6)$$

In the Introduction it was stated that the optimum profile from cavitation point of view would be the profile with constant circulation distribution over chord but that it would be difficult to incorporate this feature in a propeller. The usual propeller section is the bicircular arc profile. For this equation (6) gives immediately the camber ratio of the skeleton line. The condition of shock free entry is defined for the circular arc section as

$$\alpha_{eff} = \alpha_{geom} - \alpha_i = 0 \qquad \ldots(7)$$

which/

which means that the lift is produced by the camber ratio only;

$$C_L = \left(\frac{dC_L}{d\alpha}\right)_\infty \frac{2f_{eff}}{c} = \left(\frac{dC_L}{d\alpha}\right)_\infty \left(\frac{2f_{geom}}{c} - \frac{2f_1}{c}\right)$$

$$C_L = \left(\frac{dC_L}{d\alpha}\right)_\infty k \frac{2f_{geom}}{c} \qquad \ldots(8)$$

The factor k is called camber correction factor and gives the reduction of lift caused by the curvature of the streamline

$$k = \frac{f_{eff}}{f_{geom}} \qquad \ldots(9)$$

The circulation distribution over the chord for the circular arc section at shock free entry is not rectangular but elliptic. However, for the subsequent considerations this elliptic distribution is replaced by a rectangular one which gives the same downwash derivative at the midpoint and has the same integral value as the elliptic one. Since the aim of the theory is to determine the downwash derivative at the midpoint or the curvature of the flow there and not the exact downwash distribution over the chord this simplifying assumption regarding the circulation distribution over the chord seems reasonable. Furthermore it seems sufficient that the downwash derivative for both the elliptic and the replacing rectangular distribution should agree in two-dimensional flow (see Figure 2).

The chord of the elliptic distribution g_1 is c; the chord of the replacing rectangular distribution g_2 is $\bar{c}$. They have the same integral value if

$$\int_{-\frac{c}{2}}^{\frac{c}{2}} g_1(0) = \bar{c} g_2(0) \qquad \ldots(10)$$

where $g_1(0)$ and $g_2(0)$ are the corresponding values at the midpoint. These distributions provide the same downwash derivative in two-dimensional flow if

$$\frac{g_1(0)}{c} = \frac{g_2(0)}{\pi} \frac{\frac{\bar{c}}{2}}{\left(\frac{\bar{c}}{2}\right)^2 - x^2} \qquad \ldots(11)$$

From/

From (10) and (11) for $x = 0$

$$\frac{\bar{c}}{c} = \sqrt{0.5} = 0.707 \qquad \ldots(12)$$

The blade with circular arc sections and chord distribution c is thus replaced by a reduced blade with chord distribution $\bar{c}$ and having constant circulation distribution over the chord (see Figure 3).

3. The Vortex Surface of the Aerofoil with Constant Chordwise Circulation Distribution

The vortex surface of the aerofoil with circulation distribution $\Gamma(y)$ is covered by vortex filaments in both span and chord directions called g_y and g_x vortices. If the circulation distribution over the chord $\bar{c}$ is assumed constant then the intensity of the g_y vortices is

$$g_y = \frac{\Gamma(y)}{\bar{c}(y)} \qquad \ldots(13)$$

Since vortex filaments can only begin and end at infinity in the absence of solid surfaces (zero divergence),

$$\frac{\partial g_x}{\partial x} = -\frac{d}{dy} g_y = -\frac{d}{dy}\left(\frac{\Gamma}{\bar{c}}\right) \qquad \ldots(14)$$

For the same reason the vortex component normal to the aerofoil outline in the plane of the surface must vanish over the leading edge while over the trailing edge the component of the bound vortices normal to the outline must equal the component of the trailing vortices normal to the outline. The circulation of this vortex filament along the aerofoil outline is (see Figure 4)

$$\frac{\Gamma}{\bar{c}}\,dx = \frac{\Gamma}{\bar{c}} \frac{d\frac{\bar{c}}{2}}{dy}\,dy = \frac{\Gamma}{\bar{c}} \frac{\bar{c}'}{2}\,dy \qquad \ldots(15)$$

and it varies with y. The dash denotes a derivative with respect to y. This is the initial value of the g_x vortices which start at the leading edge. At the trailing edge their value sums up to

$$g_{xtr} = -\int_{-\frac{\bar{c}}{2}}^{\frac{\bar{c}}{2}} \frac{d}{dy}\left(\frac{\Gamma}{\bar{c}}\right) dx - C(y)$$

$$= -\int_{-\frac{\bar{c}}{2}}^{\frac{\bar{c}}{2}} \frac{d}{dy}\left(\frac{\Gamma}{\bar{c}}\right) dx - \frac{\Gamma}{2\bar{c}}\bar{c}' - \frac{\Gamma}{2\bar{c}}\bar{c}' \qquad \ldots(16)$$

with/

with the second term contributed by the vortex along the leading edge (equation 15) and the third term by that along the trailing edge. Thus

$$g_{xtr} = -\bar{c}\left[\frac{\Gamma'}{\bar{c}} - \frac{\Gamma\bar{c}'}{\bar{c}^2}\right] - \frac{\Gamma\bar{c}'}{\bar{c}} = -\Gamma'$$

and this is the value of the trailing vortices.

4. The Vortex Surface of the Propeller with Constant Chordwise Circulation Distribution

The surface of the propeller blade is part of a screw surface. The chords are arcs of helices and along their continuation behind the blade lie the trailing vortices. These helices are given by their pitch angle

$$\tan\beta = \frac{v}{r\omega} = \frac{\lambda}{x} \qquad \ldots(17)$$

where v is the forward speed, r the radius, ω the angular velocity, λ the advance ratio, and $x = \frac{r}{R}$ the dimensionless radius. According to Prandtl the pitch angle of the trailing vortices is in second approximation $\arctan \lambda_i/x_i$ where λ_i is the induced advance ratio. Therefore throughout the following investigation λ might be replaced by λ_i.

These helical lines form one set of components of vorticity. The other ones are vortices which coincide with the radii of the screw surface. The vortex surface of the aerofoil is built up by rectangles (see Figure 4), characterised by the circulation and the chord at section y. The vortex surface of the propeller blade is built up by cylindrical screw surfaces. These are sectors of a circle in the disc plane (see Figure 5). These elements of the lifting surface are characterised by the circulation at radius r and the angle τ of the disc plane at radius r. This function $\tau(r)$ replaces the function $c(y)$ of the aerofoil. The chord of the blade at section $x = \frac{r}{R}$ is related to $\tau(r)$ by

$$c = \frac{Rx\tau}{\cos\arctan\frac{\lambda}{x}} = R\tau\sqrt{x^2+\lambda^2} \qquad \ldots(18)$$

The reduced chord length $\bar{c}$ introduced in section 2 gives a reduced angle $\bar{\tau}$. Figure 6 shows the propeller blade built up by cylindrical screw elements. For constant circulation distribution over the chord the strength of the g_r vortices is

g_r/

$$g_r = \frac{\Gamma(r)}{\bar{\tau}(r)} = \frac{\Gamma(x)}{\bar{\tau}(x)} \qquad \ldots(19)$$

and that of the g_ϕ vortices (ϕ being the angular co-ordinate) is

$$\frac{\partial g_\phi}{\partial \phi} = -\frac{d}{dx}\left(\frac{\Gamma}{\bar{\tau}}\right) \qquad \ldots(20)$$

or corresponding to (16) by integration

$$g_\phi = -\frac{d}{dx}\left(\frac{\Gamma}{\bar{\tau}}\right)\phi - \frac{\Gamma\bar{\tau}'}{2\bar{\tau}} \quad -\frac{\bar{\tau}}{2} \leq \phi \leq \frac{\bar{\tau}}{2} \qquad \ldots(21)$$

The element of arc of the chord is

$$ds = \frac{Rxd\phi}{\cos \arctan \frac{\lambda}{x}} = Rd\phi\sqrt{x^2 + \lambda^2} \qquad \ldots(22)$$

5. First Part of the Downwash Derivative

The aim of the investigation is to find the downwash derivative in chord direction $dw_d/d\phi$ at a point $\phi = \phi^*$, $x = x^*$ produced by the surface of vorticity represented by the radial vortex system g_r (equation 19) and the helical vortex system g_ϕ (equation 21). The induced velocity of these vortices is given by the law of Biot-Savart in the general form (see Figure 7)

$$dw_d = \frac{1}{4\pi}\frac{G \sin \psi}{a^2} ds \qquad \ldots(23)$$

G is the circulation of the vortex line with element of arc ds at the point Q, a is the distance from the pivotal point P to the point Q, ψ is the angle between the element ds and PQ. The induced velocity is perpendicular to the plane given by ds and P. To determine the induced angle and induced camber only the component perpendicular to the screw surface at point P is needed. Therefore introduce the angle θ between the normal to the screw surface at point P and the direction of the induced velocity at this point.

For the purpose of calculation it is convenient to consider the downwash w_d as made up of three parts. The first is that produced by the g_r vortices and the g_ϕ vortices of strength given by the second term in (21). The second by the downwash produced by the g_ϕ vortices of strength given by the first term in (21). And the third part is that associated with vortices of the other blades.

Firstly/

Firstly then the radial vortices (equation 19) are considered which produce the dimensionless downwash component

$$\frac{1}{4\pi v}\int \frac{\Gamma}{\bar{\tau}}\frac{\sin\psi_1}{a^2}\cos\theta_1 ds_1 \qquad \ldots(24)$$

where s_1 is the radial co-ordinate. Secondly part of the helical vortices are considered (see equation 21) producing the downwash component

$$-\frac{1}{4\pi v}\int \frac{\Gamma\bar{\tau}'}{2\bar{\tau}}\frac{\sin\psi_2}{a^2}\cos\theta_2 ds_2 \qquad \ldots(25)$$

where s_2 is the helical co-ordinate.

Now consider the vortices ds_1 and ds_2 at the arbitrary point $\theta\,(x, \phi)$ (see Figure 8). The angle ψ_1 is the angle between PQ and the radius through Q. Imagine a system of orthogonal co-ordinates with radius OP as first axis, propeller axis as third axis and the second axis perpendicular to these two. The radius NQ in this system has direction cosines

$$\begin{aligned}\cos\mu_1 &= \cos(\phi^* - \phi)\\ \cos\nu_1 &= \sin(\phi^* - \phi)\\ \cos\tau_1 &= 0\end{aligned} \qquad \ldots(26)$$

and PQ has direction cosines

$$\begin{aligned}\cos\mu_2 &= \frac{x\cos(\phi^* - \phi) - x^*}{a}\\ \cos\nu_2 &= \frac{x\sin(\phi^* - \phi)}{a}\\ \cos\tau_2 &= \frac{\lambda(\phi^* - \phi)}{a}\end{aligned} \qquad \ldots(27)$$

and a itself is given by

$$\frac{a^2}{R^2} = x^2 + x^{*2} - 2xx^*\cos(\phi^* - \phi) + \lambda^2(\phi^* - \phi)^2 \qquad \ldots(28)$$

The/

The direction cosines of the normal to a plane containing the two directions μ_1, ν_1, τ_1 and μ_2, ν_2, τ_2 which form the angle ψ_1 between them are (see Bell "Co-ordinate Geometry of three Dimensions", pp. 22, 39)

$$\cos \mu_4 = \frac{\cos \nu_1 \cos \tau_2 - \cos \nu_2 \cos \tau_1}{\sin \psi_1} = \frac{\lambda (\phi^* - \phi) \sin (\phi^* - \phi)}{a \sin \psi_1}$$

$$\cos \nu_4 = \frac{\cos \tau_1 \cos \mu_2 - \cos \tau_2 \cos \mu_1}{\sin \psi_1} = \frac{-\lambda (\phi^* - \phi) \cos (\phi^* - \phi)}{a \sin \psi_1} \quad \ldots(29)$$

$$\cos \tau_4 = \frac{\cos \mu_1 \cos \nu_2 - \cos \mu_2 \cos \nu_1}{\sin \psi_1} = \frac{x^* \sin (\phi^* - \phi)}{a \sin \psi_1}$$

The normal to the propeller surface at P has direction cosines

$$\cos \mu_3 = 0$$

$$\cos \nu_3 = - \sin \beta_{x^*} = - \frac{\lambda}{\sqrt{x^{*2} + \lambda^2}} \quad \ldots(30)$$

$$\cos \tau_3 = \cos \beta_{x^*} = \frac{x^*}{\sqrt{x^{*2} + \lambda^2}}$$

with $\beta_{x^*} = \arctan \frac{\lambda}{x^*}$, pitch angle at P. Therefore

$$\cos \theta_1 = \cos \mu_3 \cos \mu_4 + \cos \nu_3 \cos \nu_4 + \cos \tau_3 \cos \tau_4$$

$$= \frac{\lambda^2 (\phi^* - \phi) \cos (\phi^* - \phi) + x^{*2} \sin (\phi^* - \phi)}{a \sin \psi_1 \sqrt{x^{*2} + \lambda^2}}$$

From (24) with $ds_1 = R dx$ the whole system of radial vortices gives the downwash component

$$\frac{1}{4\pi v} \int\int \frac{\Gamma}{\tau} \frac{\sin \psi_1}{a^2} \cos \theta_1 \, ds_1 \, d\phi$$

$$= \frac{1}{2\pi} \int_0^1 \int_{-\frac{\tau}{2}}^{\frac{\tau}{2}} \frac{\gamma}{\tau} \frac{\lambda^2 (\phi^* - \phi) \cos (\phi^* - \phi) + x^{*2} \sin (\phi^* - \phi)}{[x^2 + x^{*2} - 2xx^* \cos (\phi^* - \phi) + \lambda^2 (\phi^* - \phi)^2]^{3/2} \sqrt{x^{*2} + \lambda^2}} \, d\phi dx \quad \ldots(31)$$

where/

where

$$y = \frac{\Gamma}{vD} \qquad \ldots(32)$$

The advantage of this derivation is that the term $\sin\psi$ cancels.

To evaluate that part contributed by the helical vortices given by (25) the direction cosines of the helix with pitch angle $\arctan\frac{\lambda}{x}$ at Q are needed

$$\cos\mu_1 = \frac{-x\sin(\phi^* - \phi)}{\sqrt{x^2 + \lambda^2}}$$

$$\cos\nu_1 = \frac{x\cos(\phi^* - \phi)}{\sqrt{x^2 + \lambda^2}} \qquad \ldots(33)$$

$$\cos\tau_1 = \frac{\wedge}{\sqrt{x^2 + \lambda^2}}$$

The direction cosines of PQ are given by (27). Therefore

$$\cos\mu_4 = \frac{\cos\nu_1\cos\tau_2 - \cos\nu_2\cos\tau_1}{\sin\psi_2}$$

$$= \frac{\lambda x(\phi^* - \phi)\cos(\phi^* - \phi) - \lambda x\sin(\phi^* - \phi)}{a\sqrt{x^2 + \lambda^2}\sin\psi_2}$$

$$\cos\nu_4 = \frac{\cos\tau_1\cos\mu_2 - \cos\tau_2\cos\mu_1}{\sin\psi_2}$$

$$= \frac{\lambda(x\cos(\phi^* - \phi) - x^*) + \lambda x(\phi^* - \phi)\sin(\phi^* - \phi)}{a\sqrt{x^2 + \lambda^2}\sin\psi_2}$$

$$\cos\tau_4 = \frac{\cos\mu_1\cos\nu_2 - \cos\mu_2\cos\nu_1}{\sin\psi_2} = \frac{-x^2 + xx^*\cos(\phi^* - \phi)}{a\sqrt{x^2 + \lambda^2}\sin\psi_2}.$$

and/.

and with μ_3, ν_3, τ_3 from (30)

$$\cos\theta_2 = \cos\mu_3\cos\mu_4 + \cos\nu_3\cos\nu_4 + \cos\tau_3\cos\tau_4$$

$$= \frac{-\lambda^2[x\cos(\phi^*-\phi) - x^* + x(\phi^*-\phi)\sin(\phi^*-\phi)] - x^*x[x - x^*\cos(\phi^*-\phi)]}{a\sqrt{x^2+\lambda^2}\sqrt{x^{*2}+\lambda^2}\sin\psi_2}$$

The element of arc is

$$ds_2 = d\phi\sqrt{x^2+\lambda^2}$$

Therefore the whole system (25) gives the downwash component

$$-\frac{1}{4\pi v}\int\int\frac{\Gamma\bar{\tau}'}{2\bar{\tau}}\frac{\sin\psi_2}{a^2}\cos\theta_2\,ds_2\,dr = -\frac{1}{2\pi}\int_0^1\int_{-\frac{\bar{\tau}}{2}}^{\frac{\bar{\tau}}{2}}\frac{\gamma\bar{\tau}'}{2\bar{\tau}}\times$$

$$\times\frac{-\lambda^2[x\cos(\phi^*-\phi) - x^* + x(\phi^*-\phi)\sin(\phi^*-\phi)] - xx^*[x - x^*\cos(\phi^*-\phi)]d\phi dx}{[x^2+x^{*2}-2xx^*\cos(\phi^*-\phi)+\lambda^2(\phi^*-\phi)^2]^{3/2}\sqrt{x^{*2}+\lambda^2}} \quad \ldots(34)$$

Now add (31) to (34).

For the downwash derivative in chordwise direction the expression must be differentiated with respect to ϕ^*. Since ϕ and ϕ^* occur in the combination $\phi^* - \phi$ only the differentiation with respect to ϕ^* and the integration with respect to ϕ can be accomplished by omitting the ϕ integral and replacing ϕ by the limits $-\frac{\bar{\tau}}{2}$ and $-\frac{\bar{\tau}}{2}$. In particular for $\phi^* = 0$ the integrand is symmetrical and the following is the expression for this part of the downwash derivative

$$\frac{dw_{d_1}/v}{d\phi} = I_1 = \frac{1}{\pi}\int_0^1\frac{y}{\bar{\tau}}\times$$

$$\times\frac{\lambda^2\left(-\cos\frac{\bar{\tau}}{2} + x^{*2}\sin\frac{\bar{\tau}}{2}\right) + \frac{\bar{\tau}'}{2}\left[-\lambda^2\left(x\frac{\bar{\tau}}{2} - x^* + x\frac{\bar{\tau}}{2}\sin\frac{\bar{\tau}}{2}\right) - xx^*\left(x - x^*\cos\frac{\bar{\tau}}{2}\right)\right]}{\sqrt{x^{*2}+\lambda^2}\left[x^2+x^{*2}-2xx^*\cos\frac{\bar{\tau}}{2}+\lambda^2\left(\frac{\bar{\tau}}{2}\right)^2\right]^{3/2}}dx \quad \ldots(35)$$

This downwash derivative of the system of g_r vortices (19) and of the second term of the g_ϕ vortices (21) (which is independent of ϕ) was gained from the downwash itself by simply replacing the coordinate ϕ by its limits and dropping the integral. This shows that it can be explained as downwash itself. The downwash derivative is the

effect/

effect of the original vortex surface minus the effect of this surface moved by the differential amounts $d\phi$ or ds in chord direction. The two surfaces overlap in their main part and since the circulation distribution over the chord is constant the g_r vortices and g_ϕ vortices cancel each other with the exception of those portions at the leading edge and at the trailing edge (see Figures 3 and 4). The remaining parts of both systems form one continuous vortex which has the shape of the (reduced) blade outline. This is the physical explanation for associating the contributions from the g_r vortices (equation 19) and from the second part of the g_ϕ vortices (equation 21). Equation (35) gives the downwash at $P(\phi^*, x^*)$ from the circumferential vortex of strength $\frac{y}{\bar{\tau}} d\phi$ (see Figure 9). This is the first part of the downwash derivative. Strassl[2] gave another derivative of equation (35) starting from the circumferential vortex but this derivation is less simple than that given above in equations (26) to (35). In the original report[1] a more geometrical method was used whereas present equation (35) proved the more accurate and was first used in Strassl's calculations.

6. Second Part of the Downwash Derivative

The velocity induced at point P by the first term in (21) of the helical vortices g_ϕ

$$-\frac{d}{dx}\left(\frac{\Gamma}{\bar{\tau}}\right)\phi \qquad -\frac{\bar{\tau}}{2} \le \phi \le \frac{\bar{\tau}}{2}$$

can be written as

$$= -\frac{1}{2\pi}\int_0^1 \int_{-\frac{\bar{\tau}}{2}}^{\frac{\bar{\tau}}{2}} \frac{d}{dx}\left(\frac{y}{\bar{\tau}}\right)(\phi - \phi^*)\,\frac{dK\,(\phi - \phi^*,\, x,\, x^*)}{d\phi}\,d\phi dx \qquad \ldots(36)$$

Here

$$\iint \frac{dK}{d\phi}\,d\phi dx$$

is the induced velocity for such vortices of unit strength. Partial integration with respect to ϕ gives

$$= -\frac{1}{2\pi}\int_0^1 \frac{d}{dx}\left(\frac{y}{\bar{\tau}}\right)(\phi - \phi^*)\,\Big[K\Big]_{-\frac{\bar{\tau}}{2}}^{\frac{\bar{\tau}}{2}} dx + \frac{1}{2\pi}\int_0^1 \int_{-\frac{\bar{\tau}}{2}}^{\frac{\bar{\tau}}{2}} \frac{d}{dx}\left(\frac{y}{\bar{\tau}}\right) K(\phi - \phi^*,\, x,\, x^*)\,d\phi dx$$

If the derivative with respect to ϕ^* is taken the first term vanishes for reasons of symmetry for $\phi^* = 0$. The downwash is the component of the induced velocity perpendicular to the screw surface, therefore as before a factor $\cos\theta$ must be added. Then the second term gives the downwash

$$\frac{w_a}{v}$$

$$\frac{w_{d_2}}{v} = \frac{1}{2\pi}\int_0^1 \frac{d}{dx}\left(\frac{\gamma}{\bar{\tau}}\right)\int_{-\frac{\bar{\tau}}{2}}^{\frac{\bar{\tau}}{2}} K\,(\phi - \phi^*,\ x,\ x^*)\cos\theta\ d\phi dx$$

Differentiation with respect to ϕ^* and integration with respect to ϕ gives, when $\phi^* = 0$, by reason of symmetry, for the downwash derivative

$$\frac{dw_{d_2}/v}{d\phi} = I_2 = -\frac{1}{\pi}\int \frac{d}{dx}\left(\frac{\gamma}{\bar{\tau}}\right) K\left(\frac{\bar{\tau}}{2},\ x,\ x^*\right)\cos\theta\ dx \qquad \ldots(37)$$

where K is the induced velocity for a vortex of unit strength along the helical line between leading and trailing edge and θ is as before the angle between the velocity induced by the vortex through Q and the normal to the screw surface at the point P. Equation (37) shows that the second part of the downwash derivative can be explained as downwash of a surface of helical vortices connecting the leading and the trailing edges and having the strength $-\frac{d}{dx}\left(\frac{\gamma}{\bar{\tau}}\right) d\phi$ (see Figure 9).

The rest of this section is devoted to the kernel K. The helical arcs of length $\bar{c} = R\bar{\tau}\sqrt{x^2 + \lambda^2}$ appear in the disc plane as circular arcs $Rx\bar{\tau}$. These helical arcs may be replaced by circular arcs of angle $\bar{\tau}$ and of radius

$$R\bar{x} = R\sqrt{x^2 + \lambda^2} \qquad \ldots(38)$$

Since this circular arc is to pass through the midpoint of the helical arc, its centre lies beyond the axis a distance $\bar{x} - x$. The position of the pivoted point P to the circular arc is therefore given by

$$\sigma_{\bar{x}} = \frac{x^* + \bar{x} - x}{\bar{x}} \qquad \ldots(39)$$

if the radius of every circular arc is reduced to unity. This reduction has to be amended if and when the integral is taken (see equation 40).

First the integration over the elementary circular arc with (for this integration) constant circulation distribution

$$\gamma_1 = -\frac{1}{\bar{x}}\frac{d}{dx}\left(\frac{\gamma}{\bar{\tau}}\right) d\phi \qquad \ldots(40)$$

has to be considered. This can be done in terms of elliptical integrals. The radius is reduced to 1, the pivotal point is $\sigma_{\bar{x}}$. For reasons of symmetry integration over half the circular arc $\frac{\bar{\tau}}{2}$ is sufficient. In accordance with Figure 10, Biot Savart's law (23) gives as the corresponding induced velocity

$$\frac{\gamma_1}{\pi}/$$

$$\frac{\gamma_1}{\pi}\int_0^{\frac{\bar{\tau}}{2}} \frac{1-\sigma_{\bar{x}}\cos\phi'}{(1+\sigma_{\bar{x}}^2-2\sigma_{\bar{x}}\cos\phi')^{3/2}}\,d\phi'$$

where ϕ' is the angle between $O'P$ and $O'Q$, where O' is the centre of the circular arc. This integral is (see [3] p. 128)

$$\int_0^{\frac{\bar{\tau}}{2}} \frac{1-\sigma_{\bar{x}}\cos\phi'}{(1+\sigma_{\bar{x}}^2-2\sigma_{\bar{x}}\cos\phi')^{3/2}}d\phi' = \frac{2}{(1+\sigma_{\bar{x}})^2}\left[\frac{E'}{k'^2}-\left(\frac{E(\chi)}{k'^2}-\frac{k^2\sin\chi\cos\chi}{k'^2\Delta}\right)\right]$$

$$-\frac{4\sigma_{\bar{x}}}{(1+\sigma_{\bar{x}})^3}\left[\frac{F'-D'}{k'^2}-\frac{F(\chi)-D(\chi)}{k'^2}-\frac{\sin\chi\cos\chi}{k'^2\Delta}\right] \qquad \ldots(41)$$

with

$$k^2 = \frac{4\sigma_{\bar{x}}}{(1+\sigma_{\bar{x}})},\quad k'^2 = 1-k^2 = \frac{(1-\sigma_{\bar{x}})^2}{(1+\sigma_{\bar{x}})^2},\quad \chi = \frac{\pi}{2}-\frac{\bar{\tau}}{4}$$

$$D' = \frac{F'-E'}{k'^2},\quad \Delta = \sqrt{1-k^2\sin^2\chi} = \sqrt{1-k^2\cos^2\frac{\bar{\tau}}{4}} \qquad \ldots(42)$$

where

F' is the complete elliptical integral of first order

E' " " " " " " second "

F is the incomplete " " " first "

E " " " " " " second "

The term consisting of complete integrals can be written

$$\frac{2}{(1-\sigma_{\bar{x}})^2}E' - \frac{4\sigma_{\bar{x}}}{(1+\sigma_{\bar{x}})^3}\,\frac{F'-\frac{F'-E'}{k^2}}{1-k^2} = \frac{E'}{1-\sigma_{\bar{x}}}+\frac{F'}{1+\sigma_{\bar{x}}} \qquad \ldots(43)$$

and is already tabulated[4]. For the incomplete integral terms

$$-\frac{2}{(1+\sigma_{\bar{x}})^2}\,\frac{1}{1-k^2}\left[E(\chi)-\frac{k^2\sin\chi\cos\chi}{\Delta}\right]+\frac{4\sigma_{\bar{x}}}{(1+\sigma_{\bar{x}})^3}\,\frac{1}{1-k^2}\times$$

$$\times\left[F-\frac{F-E}{k^2}-\frac{\sin\chi\cos\chi}{\Delta}\right] = -\frac{1}{1-\sigma_{\bar{x}}}\left(E-\frac{k^2\sin\chi\cos\chi}{\Delta}\right)-\frac{F}{1+\sigma_{\bar{x}}}$$

Adding/

Adding these results

$$\frac{dw_{d_2}/v}{d\phi} = I_b = -\frac{1}{\pi}\int \frac{1}{\bar{x}}\frac{d}{dx}\left(\frac{\gamma}{\bar{r}}\right)\cos\theta\left[\frac{1}{1-\sigma_{\bar{x}}}\left[E' - \left[E\left(k,\frac{\pi}{2}-\frac{\bar{\tau}}{4}\right) - \frac{k^2\sin\frac{\bar{\tau}}{4}\cos\frac{\bar{\tau}}{4}}{\Delta}\right]\right] + \frac{1}{1+\sigma_{\bar{x}}}\left[F' - F\left(k,\frac{\pi}{2}-\frac{\bar{\tau}}{4}\right)\right]\right]dx \qquad \ldots(44)$$

$$\text{where} \quad \theta = \arctan\frac{\lambda}{x} - \arctan\frac{\lambda}{x^*} \qquad \ldots(45)$$

The kernel

$$K(\chi,\sigma_{\bar{x}}) = \frac{1}{1-\sigma_{\bar{x}}}\left[E'\left(k,\frac{\pi}{2}\right) - \left[E\left(k,\frac{\pi}{2}-\frac{\bar{\tau}}{4}\right) - \frac{k^2\sin\frac{\bar{\tau}}{4}\cos\frac{\bar{\tau}}{4}}{\Delta}\right]\right] + \frac{1}{1+\sigma_{\bar{x}}}\left[F'\left(k,\frac{\pi}{2}\right) - F\left(k,\frac{\pi}{2}-\frac{\bar{\tau}}{4}\right)\right] \qquad \ldots(46)$$

has been tabulated for a certain range of $\sigma_{\bar{x}}$ and χ (see Table).

7. Third Part of the Downwash Derivative

Strictly the downwash and its derivative at a point P of the propeller blade depend on the vortex systems of all the blades. So far only the vortex system of the original blade containg P has been considered. In the original report[1] the influence of the other blades has been considered in an approximate manner. But experience has shown that the numerical influence of these blades is small. At points of small radius this influence is not negligible but since the interference of the hub is completely ignored in this paper there is not much point in taking account of the former effect. Therefore in all later calculations ([2] and in this paper) the third part of the downwash derivative produced by the other blades has been neglected.

The following considerations show the plausibility of the influence being small. First of all the vortex system of Figure 9 which provides the downwash derivative may be thought of alternatively as the system shown in Figure 11. These are closed vortices of constant vorticity $-\frac{d}{dx}\left(\frac{\Gamma}{\bar{r}}\right)d\phi$. Starting at the propeller axis, any particular filament follows the outline of the blade to that point of the leading edge where the helical vortex of radius x starts, follows this helical line to the trailing edge and then back along the outline to the axis.

Now/

Now consider the influence of one such vortex filament on the second and third blades on the "downwash derivative" at the pivotal point P of the original blade (see Figure 12). Vortices 2 and 2', 3 and 3' add to the velocity at P induced by the original blade, but 1 and 1' reduce it. The influence of 1 and 1' is stronger than that of 2, 2' or that of 3, 3' since they lie nearer. The final result depends on the blade width, the number of blades and the advance ratio but these opposing influences result in a relatively small effect produced by these blades on the downwash derivative at the mid chord of the original blade.

8. The Camber Correction Factor of the Propeller Blade

Equations (6) and (8) give, for the special value $\left(\frac{dC_L}{D\alpha}\right)_\infty = 2\pi$,

$$\frac{f_{geom}}{c} = \frac{c}{8V}\frac{dw_d}{ds} \qquad \ldots(6)$$

$$C_L = \frac{2\Gamma}{Vc} = 4\pi\frac{f_{eff}}{c} \qquad \ldots(8)$$

and therefore

$$k = \frac{f_{eff}}{f_{geom}} = \frac{4\Gamma}{\pi c^2\frac{dw_d}{ds}} = \frac{4\Gamma R\sqrt{x^2+\lambda^2}}{\pi c^2\frac{dw_d}{d\phi}} \qquad \ldots(47)$$

Write the non-dimensional calculation (32)

$$\gamma = \frac{\Gamma}{vD} = A\gamma_o \qquad \ldots.(48)$$

where the A factor depends on the loading. Since the downwash derivative is proportional to A the camber correction factor is independent of the loading

$$k = \frac{\gamma_o\sqrt{x^2+\lambda^2}}{\pi\left(\frac{c}{D}\right)^2\frac{d\frac{w_d}{v}(\gamma_o)}{d\phi}} \qquad \ldots(49)$$

where/

where

$$\frac{d\,\frac{w_d}{v}\,(y_o)}{d\varphi} = I_1 + I_2 \qquad \ldots(50)$$

I_1 is given by equation (35) and I_2 by equation (44) both calculated with y_o defined by (48) instead of y.

The factor A in (48) depends on the thrust coefficient C_T of the propeller and, as a first approximation

$$A = \frac{\pi\lambda\, C_T}{4z \int_0^1 y_o\, x\, dx} \qquad \ldots(51)$$

9. The Camber Correction for Best Distribution of Circulation

The camber correction factor has been calculated assuming the best distribution of circulation over two sets of affine shapes (see Figures 13 and 14) for several different advance ratios (see Figures 15 and 16). The calculations were carried out mainly by Strassl[2]. Without going into great detail some important points should be mentioned.

The integrand J_1 (35) of I_1 has a singularity at the tip $x = 1$ tending to infinity there $\frac{1}{\sqrt{1-x}}$. Divide the integral at say $x' = 0.9$ into two parts

$$I_1 = \frac{1}{\pi}\int_0^{x'} J_1\, dx + \frac{1}{\pi}\int_{x'}^1 J_1\, dx$$

and introduce the variable

$$u = \sqrt{1-x}$$

into the second part. Then

$$\int_{x'}^1 J_1\, dx = \int_0^{u'} 2u\, J_1\, du \quad \text{with} \quad u' = \sqrt{1-x'}$$

The/

The limiting value of $2u\,J_1$ at $u = 0$ is independent of the shape of the blade, that means independent of $\bar{r}(x)$, and has the value

$$\sqrt{\frac{2}{\lambda}}\,\frac{1}{(1+\lambda^2)^{3/4}}\,\frac{\lambda^2 + x^*}{(1-x^*)^2\,\sqrt{\lambda^2 + x^{*2}}}$$

The integrand J_2 of I_2 (44) tends to infinity at $x = x^*$ with changing sign. Therefore

$$I_2 = \frac{1}{\pi}\int_0^{x^*-j} J_2\,dx + \frac{1}{\pi}\int_{x^*-j}^{x^*+j} J_2\,dx + \frac{1}{\pi}\int_{x^*+j}^{1} J_2\,dx$$

The middle integral is symmetrical to x^* and its principal value can be calculated by adding the integrands at $x^* - \epsilon$ and at $x^* + \epsilon$ symmetrical about x^*, that is

$$\int_{x^*-j}^{x^*+j} J_2\,dx = \int_0^{j} [J_2\,(x^* - \epsilon) + J_2\,(x^* + \epsilon)]\,d\epsilon$$

where $\epsilon = |x - x^*|$ varies from 0 to j. The limiting value at $\epsilon = 0$ and the limiting value of the third integrand at $x = 1$ are of less importance but can easily be calculated by developing the integrands at these points.

10. Some Remarks about Previous Theories of the Camber Correction Factor

The fact that the camber ratio calculated by means of the usual propeller theory (lifting line) is too small has been known for a long time from experimental results and several attempts have been made to provide a better theory. Helmbold[5] in 1933 gave a theoretical approach to the problem which is very much on the lines of the present paper. Since the numerical results do not agree with those given in this paper it seems worthwhile to recount briefly Helmbold's theory and to show the differences between his approach and the present one.

The axial and the tangential velocity of the propeller behave in a different manner. The change from $r\omega$ to $r\omega - w_t$ takes place almost immediately in the disc plane whereas the increase of the axial component from v to $v + w_a$ is continuous. If therefore the projection of the chord in the plane containing the radius and the propeller axis is no longer small the variation of the axial velocity has to be considered.

Designating the additional velocities by v_a and v_t and the hydrodynamical pitch angle by β with

$$\tan\beta = \frac{v + \frac{w_a}{2}}{r\omega - \frac{w_t}{2}}$$

then/

then the additional velocity normal to the mean inflow velocity V is

$$w_d = v_a \cos\beta + v_t \sin\beta$$

Then in accordance with equation (4) the radius of curvature R_c of the streamline is given by

$$\frac{1}{V}\frac{dw_d}{ds} = \frac{1}{R_c} = \frac{1}{V}\left(\frac{\partial v_a}{\partial s}\cos\beta + \frac{\partial v_t}{\partial s}\sin\beta\right) \qquad \ldots(52)$$

where ds is the element of the streamline. The two terms are now considered separately.

Assuming that the increase of v_t takes place in the propeller plane, Helmbold considers that it is satisfactory to calculate this part by the cascade theory. The cascade theory being a two-dimensional theory certainly does take account only of the increase of v_t (due to the influence of the other blades). Helmbold refers to calculations by Weinig and Numachi who gave a correction factor k to the lift coefficient putting

$$\Gamma = k\, C_L\, V\, \frac{c}{2}$$

where k depends on the local pitch angle and changes sign at $\beta = \frac{\pi}{4}$.

Helmbold then calculates the derivative of the additional axial velocity v_a by replacing the propeller flow by the non-rotating slipstream with constant axial velocity over the radius. Then the slipstream is represented by the parallel inflow v plus the influence of a semi-infinite vortex cylinder of radius R. The derivative in streamline direction is the derivative in axial direction e multiplied by $\sin\beta$. Therefore the first term of (52)

$$\left[\frac{1}{R_c}\right]_{v_a} = \frac{1}{V}\frac{\partial v_a}{\partial e}\sin\beta\cos\beta \qquad \ldots(53)$$

The differential in axial direction is the influence of the original semi-infinite vortex cylinder minus the influence of a similar vortex cylinder moved by the infinitesimal distance de. In the limit the difference between these two vortex cylinders is a vortex ring of radius R in the propeller plane and of strength

$$\frac{d\Gamma}{de} = w_a$$

The/

The required downwash derivative in axial direction at radius r is given by the velocity induced by a vortex ring of radius R and of strength $\frac{d\Gamma}{de}$ at a point of radius r in its own plane. This induced velocity can be expressed by complete elliptic integrals (see equation (43)) giving

$$\frac{\partial v_a}{\partial e} = \frac{w_a}{\pi R} \frac{E}{1 - x^2}$$

This derivation strictly holds only for the propeller with infinite number of blades and with constant induced axial velocity over the radius. Helmbold applies it to the propeller with finite number of blades and with variable axial velocity by introducing κw_a instead of w_a, where κ is the Goldstein factor, accordingly

$$\left[\frac{1}{R_c}\right]_{v_a} = \frac{1}{V} \frac{\kappa w_a}{\pi R} \frac{E(x) \sin\beta \cos\beta}{1 - x^2}$$

Therefore finally (see equation (5))

$$\Gamma = k \frac{dC_L}{d\alpha} V \frac{c}{2} \left[\alpha - \frac{c}{4\pi R} \frac{\kappa w_a}{V} \frac{E(x) \sin\beta \cos\beta}{1 - x^2} \right]$$

The basic idea behind the method of the present paper is almost the same as that of Helmbold's paper, but his simplifications are not introduced. The axial velocity of the best propeller is not constant along the radius and Figure 31 shows, for example, that the camber correction factor does depend on the circulation distribution. Helmbold's calculation makes the downwash derivative independent of the shape and this is certainly not true. Furthermore if a lifting surface is used the v_t velocity varies along the chord by the influence of the bound vortices of the blade itself. Numerical agreement between Helmbold's results and the present ones therefore cannot be expected.

11. Limiting Cases. Downwash Derivative and Camber Correction Factor for the Aerofoil with Shock Free Entry at the Leading Edge

The theory developed in previous sections is an approximate theory of the lifting surface. Its validity therefore can be checked to a certain extent by comparison with exact aerofoil theories. The exact calculation of the lifting surface has only been carried out for the circular and elliptic discs[6,7], and for the cap of a sphere with zero angle of incidence[6]. Since the present method for the camber correction is developed for zero effective angle of incidence (shock free entry) only, it is the case of the cap of a sphere that is suitable for comparison. Kinner has shown that the circulation distribution over span is parabolic in this case

$$\Gamma \propto 1 - \eta^2$$

so that

$$\frac{\Gamma}{c} \propto \sqrt{1 - \eta^2} \qquad \ldots(54)$$

where/

where η is the spanwise co-ordinate. The downwash derivative is obtained from the velocity induced by the circumferential vortex of strength $\frac{\Gamma}{c}$ and by the vortex layer of strength $\frac{d}{dy}\left(\frac{\Gamma}{c}\right)$ running in flow direction from the leading edge to the trailing edge. As long as the strength of the circumferential vortex remains finite at the tip the downwash derivative must tend to infinity at the tip; this point will be discussed in detail later. For the cap of the sphere however, $\frac{\Gamma}{c}$ tends to zero at the tip according to (54).

From equation (5), a constant downwash derivative along the span can be expected if

$$\frac{f}{c^2} = \frac{1}{8V}\frac{dw_d}{dx} = \text{const.} \qquad \ldots(55)$$

Presupposing elliptic outline this condition is fulfilled for the small cap of an ellipsoid of revolution and therefore this case was considered in more detail. Since from (54) $\frac{\Gamma}{c^2}$ is constant, the camber correction factor will also be constant from (47). The actual calculation[8] is very cumbersome, several principal values of integrals having to be calculated, but the result is independent of y and is given by the simple relation

$$\frac{dw_d}{dx} = \frac{1}{\pi a^2} + \frac{1}{4\pi\sqrt{1-\frac{a^2}{2}}}\ln\frac{1+\sqrt{1-\frac{a^2}{2}}}{1-\sqrt{1-\frac{a^2}{2}}} \qquad \ldots(56)$$

where a is the axis ratio

$$a = \frac{c(0)}{b}$$

of the elliptic outline of the wing. Then the corresponding camber correction factor

$$k = \frac{1}{1 + \frac{a^2}{4\sqrt{1-\frac{a^2}{2}}}\ln\frac{1+\sqrt{1-\frac{a^2}{2}}}{1-\sqrt{1-\frac{a^2}{2}}}} \qquad a < 1 \qquad \ldots(57a)$$

or/

or

$$k = \frac{1}{1 + \dfrac{a\sqrt{2}}{2\sqrt{1 - \dfrac{2}{a^2}}\arcsin\sqrt{1 - \dfrac{2}{a^2}}}} \qquad a > 1 \qquad \ldots(57b)$$

If $a \to 0$, k tends to 1 in accordance with (57a), and this is the limiting case of the lifting line.

If $a \to \infty$, k tends to zero, but the lift itself has a finite limiting value. The total lift coefficient is

$$\bar{C}_L = \frac{1}{\pi a} 4\pi k \int_{-1}^{+1} f(\eta)\, d\eta = \frac{4k}{a} f(0) \int_{-1}^{+1} (1 - \eta^2)\, d\eta = \frac{16k}{3a} f(0)$$

whence the total lift is given by, using (57b)

$$\frac{L}{\rho V^2 b^2 \dfrac{2f(0)}{c(0)}} = \frac{2\pi}{3\left[\dfrac{1}{a} + \dfrac{1}{\sqrt{2\left(1 - \dfrac{2}{a^2}\right)}}\arcsin\sqrt{1 - \dfrac{2}{a^2}}\right]} \qquad \ldots(58)$$

Hence

$$\lim_{a\to\infty} \frac{L}{\rho V^2 b^2 \dfrac{2f(0)}{c(0)}} = \frac{4}{3}\sqrt{2} = 1.88$$

For the cap of the sphere $a = 1$, the result is

$$\frac{dw_d}{dx} = 0.517, \quad k = 0.615$$

The coefficient of total lift for this "cap" (twisted so that the condition of shock free entry is fulfilled everywhere along the span) becomes

$$\bar{C}_L = 3.27\, f(0)$$

From this it was estimated[8] that the total lift coefficient for the untwisted cap with zero angle of incidence would be

$$\bar{C}_L = 1.75\, f(0)$$

while/

while Kinner gives

$$\tilde{c}_L = 1.87\, f(0)$$

Equation (57) gives a general idea of the dependence of the camber correction factor on the aspect ratio (see Figure 17) $\frac{dw_d/v}{ds}$ decreases with increasing $\frac{c}{b}$ but $c^2 \frac{dw_d/v}{ds}$ increases and therefore k decreases according to (47). The dotted curve in Figure 17 refers to a constant circulation distribution over rectangular wings. Here, however, the camber correction is not constant along the span, so the curve refers only to one point of the span but it shows the same tendency of k with aspect ratio.

For the elliptic outline the parabolic circulation distribution ("cap" of the ellipsoid of revolution with shock-free entry) was found to be the only one with constant downwash derivative (and constant camber correction) along the span. The function $\frac{\Gamma}{c}$ is elliptic in this case. Figure 18 shows that this is the important feature, because for the rectangle with elliptic circulation distribution the downwash derivative along span proves to be constant as well. The figure gives the three cases

$$\frac{\Gamma}{c} = 1, \quad \frac{\Gamma}{c} = \sqrt{1-\eta^2} \quad \text{and} \quad \frac{\Gamma}{c} = 1-\eta^2$$

for the two outlines circle and square. The similarity is striking.

The corresponding camber correction factors are given in Figures 19 and 20. For the square with elliptic circulation distribution $\frac{\Gamma}{c}$ is elliptic giving a constant downwash derivative, but $\frac{\Gamma}{c^2}$ is not constant, so that neither is k in this case.

12. Influence of Blade Shape, Number of Blades and Circulation Distribution on the Camber Correction for the Propeller

So far the camber correction factor had only been calculated for best distribution over two sets of affine outlines[2] (see Figures 13 and 14). The downwash derivative decreases with increasing blade area (see Figures 21 and 22) but $c^2 \frac{dw_d}{d\phi}$ increases and therefore in accordance with equation (47) k decreases (see Figures 15 and 16). If the total blade area is distributed over say 6 blades instead of over 3, the width of the single blade of the 6 bladed propeller is only half that of the latter. Therefore the camber correction factor would increase from points on say the 100% curve to those on the 50% curve (Figures 15 and 16) which means that the necessary geometrical camber ratios of the 6 bladed propeller are smaller than those of the 3 bladed one. For points near the tip where k is small (impracticably high geometrical camber ratios) the increase of number of blades might be the only way to achieve the required lift for these points.

Besides/

Besides the two sets of shapes in Figures 13 and 14 the k factor has been calculated for some elliptic blades (see Figure 23). Generally the k factor seems to decrease if the maximum width of the blade shifts towards the tip, (see Figures 24, 25 and 26).

For the case of the hydrofoil a simple rule relating the downwash derivative with the ratio of the circulation to the chord was noted (Section 11 and Figure 18). A similar correspondence exists for the propeller as is shown by Figure 27. The shape corresponding to the rectangular hydrofoil is the sector shaped propeller blade since this has a constant angle τ (see Figure 5) corresponding to constant chord length in the hydrofoil. Shape 2 (Figure 14) is nearly sector-shaped.

The dependence of the camber correction factor on the advance ratio or on the pitch is given in Figures 15, 16, 28. This dependence on λ seems to become very slight if the projected shape is held constant rather than the developed shape. However, this was only demonstrated for a very simple case, viz., for the sector blade with constant circulation distribution (Figure 29).

For this simple shape the first attempts were made with a circulation distribution different from the best distribution (Figure 30 and 31). For reasons of comparison the camber correction for best distribution as well is given using Lock's approximation

$$\Gamma_{opt} = Ax\sqrt{1 - x^2}$$

where A was chosen equal to 3 in order to provide the integral $\int\Gamma(x)\,dx = 1$ for comparison with the constant distribution $\Gamma(x) = 1$. The best distribution gives an almost constant downwash derivative because $-\frac{\Gamma}{\tau}$ is almost elliptic in this case; this is discussed in detail later in Section 15.

13. The Shape of the Blade with Minimum Surface Cavitation

To obtain maximum thrust for a given blade area while avoiding surface cavitation, the drop in pressure should be constant over the back of the blade. To provide nearly constant pressure over chord shock free entry at the leading edge is needed and the necessary lift is produced by the camber of the profile only. Considering a circular arc camber line the minimum pressure over the back occurs at the midpoint of the profile and it should be arranged that this is constant over the radius.

The difference between the minimum pressure p_{min} and the static pressure p_o is given by the maximum velocity v_{max} over the profile and the inflow velocity V to it as

$$p_o - p_{min} = \frac{\rho}{2}(v_{max}^2 - V^2) \qquad \ldots(59)$$

For/

For circular arc profiles of camber ratio $\frac{f_{eff}}{c}$ and maximum thickness t this difference is given by

$$p_o - p_{min} = \frac{\rho}{2}(v_{max}^2 - V^2) = \frac{\rho}{2} V^2 \left(\frac{8 f_{eff}}{c} + \frac{8}{\pi} \frac{t}{c} \right) = \frac{\rho}{2} v^2 \sigma_o \qquad \ldots(60)$$

where v is the forward velocity and σ_o the corresponding cavitation number. The first term in the third expression is mainly the lift coefficient C_L since by (8) and (32)

$$C_L = \frac{4\pi f_{eff}}{c} = \frac{2\Gamma}{Vc} = \frac{2y\lambda}{\sqrt{x^2 + \lambda^2}\,\frac{c}{D}} \qquad \ldots(61)$$

Then (60) becomes

$$\frac{\pi}{4}\sigma_o = \frac{x^2 + \lambda^2}{\lambda^2} \left[\frac{\lambda y}{\sqrt{x^2 + \lambda^2}\,\frac{c}{D}} + \frac{2\frac{t}{D}}{\frac{c}{D}} \right] \qquad \ldots(62)$$

Therefore the shape which provides uniform pressure drop along the radius is

$$\frac{c}{D} = \frac{4}{\pi\sigma_o \lambda} \left[\sqrt{x^2 + \lambda^2} + \frac{x^2 + \lambda^2}{\lambda} 2 \frac{t}{D} \right] \qquad \ldots(63)$$

The first expression on the right hand side depends on the circulation distribution and on the loading C_T, for the second one the general expression

$$\frac{t}{D} = 0.04\,(1 - x)$$

seems to cover the thickness distributions which are generally provided. Introducing (48) and (51)

$$\frac{c}{D} = \frac{4}{\pi\sigma_o} \left[\frac{\pi C_T}{4z \int_o^1 y_o x dx} \sqrt{x^2 + \lambda^2}\; y_o \frac{x^2 + \lambda^2}{\lambda^2} 0.08\,(1 - x) \right] \qquad \ldots(64)$$

if v is constant then $\frac{c}{D}$ is (for given σ_o) given by (64), if $R\omega$ is constant the factor λ^2 must be added.

For/

For the best distribution of circulation

$$y_o = \frac{\kappa x^2}{x^2 + \lambda^2} \qquad \ldots(65)$$

the corresponding blade shapes for the first case are given in Figure 32. The dotted curve is the fraction arising from the thickness distribution which cannot be neglected, especially for small loadings. The resulting blade shapes are approximately affine and are very similar to Shape 1 used in Ref. 2 (see Figure 13). Therefore this shape is the most useful for avoiding surface cavitation provided that the best distribution of circulation is employed.

For shock free entry the pitch angle of the chord (see Figure 33) is the induced angle of advance

$$\theta_c = \beta + \alpha_i \qquad \ldots(66)$$

and the pitch angle of the zero lift line separates into two parts

$$\theta = \theta_c + \alpha_o$$
$$\alpha_o = \frac{2f_{eff}}{c} = \theta - (\beta + \alpha_i) \qquad \ldots(67)$$

The first part θ_c is independent of the shape and depends on the circulation distribution only. The second part depends on the shape as well.

The following investigations are based on an example

$$C_T = 0.327 \quad \sigma_o = 0.98 \quad \lambda = 0.2 \quad z = 3$$

The blades corresponding to (64) are compared with a circular blade and have the same blade area.

The best distribution of circulation is the only one in which the shock free entry chord lines form a constant pitch screw surface since the condition for minimum loss of kinetic energy is

$$x \tan (\beta + \alpha_i) = \text{const.} \qquad \ldots(68)$$

For any other circulation distribution $x \tan \theta_c$ is no longer constant and the blade is twisted.

In addition to the best distribution, two other circulation distributions are considered, one with finite slope at the tip and the other one with zero slope at the tip. Though the downwash of the lifting line theory given by the principal value of an integral is no longer convergent at the tip itself (logarithmic singularity) for

circulation/

circulation distributions with finite slope, this is a mere mathematical difficulty of the lifting line theory and no physical singularity of the downwash induced by the lifting surface. In particular using a method like Multhopp's[9] the difficulty is overcome by the mechanical integration giving reasonable values for the downwash up to the point 0.981 nearest to the tip.

The particular examples chosen are

$$y = \frac{\pi\lambda C_T}{4z}\,\frac{\kappa x^2}{0.352\,x^2 + \lambda^2} \qquad \ldots(69a)$$

$$y = \frac{\pi^2\lambda C_T}{4z}\sin x\pi \qquad \ldots(69b)$$

$$y = \frac{2\pi\lambda C_T}{4z}\left(1 + \sin\left(4x - 1\right)\frac{\pi}{2}\right) \qquad \ldots(69c)$$

The corresponding blade shapes are given by (63) and are plotted in Figures 34a, 34b, 34c; the effective camber ratios as given by (66) and plotted in Figures 35a, 35b, 35c and the critical cavitation numbers are given by (60) and plotted in Figures 36a, 36b, 36c. To show the twist of the blades the expression $x \tan(\beta + \alpha_i)$ is plotted in Figures 37a, 37b, 37c.

The effective camber ratio is proportional to the lift coefficient. In all three cases (see Figure 35) the adequate blade (i.e., p_{min} = constant) provides high lift coefficients near the hub which decrease towards the tip; the figures do of course refer to idealized propellers without hubs. The elliptic blade produces a much more uniform distribution of lift coefficient over radius in the case (a) of best distribution.

Figure 38 shows the thrust distribution for the cases (a), (b), (c). Any derivation from the best distribution entails a loss of efficiency but this loss is surprisingly small in view of the considerable change of distribution (b) and (c) from that of (a).

14. The Impossibility of Achieving Exactly Constant Suction over the Whole Blade

In the previous section it was shown that the condition of shock free entry settles the pitch distribution of the blade (see equation 65) and that the condition of uniform minimum pressure over back settles the shape of the blade (see equation 63). The effective camber ratio is determined by the circulation distribution (see equation 61). The corresponding geometrical camber ratio is related to the downwash derivative of the streamline by equation (6). In sections 5 and 6 it was seen that the downwash derivative is determined directly from the actual downwash of a remainder vortex system, viz., that consisting of a single vortex which has the form of the blade outline (with chord reduced by a factor $\frac{1}{2}\sqrt{2}$) and has the strength $\frac{\Gamma}{\tau}$ and a system of vortices covering the blade in chord

direction/

direction and having the strength $\frac{d}{dx}\left(\frac{\Gamma}{\tau}\right) dx$ where τ, $\bar{\tau}$ are related to the chords c, $\bar{c}$ by (18). Therefore the required downwash derivative tends to infinity as $1/(1 - x)$ at the tip as long as $\frac{\Gamma}{\tau}$ or $\frac{\Gamma}{c}$ tends to a finite limit there. Unfortunately this is in fact the case for the adequate shape defined by (63) since from (63) and (18)

$$\frac{y}{\tau} = \frac{y\sqrt{x^2 + \lambda^2}}{\frac{c}{2 - \frac{8}{\pi\varpi_0\lambda}}} = \frac{y}{\left[\frac{\sqrt{x^2 + \lambda^2}}{\lambda y} + 0.08\,(1 - x)\right]}$$

Since in practical cases the second term in the denominator vanishes near the tip, $\frac{y}{\tau}$ is finite there. Hence from (6) the geometrical camber ratio tends to infinity if the chord vanishes at a lower order than $1 - x$. It is impossible in this case to provide the camber necessary to maintain the design circulation near the tip. That is to say a uniform distribution of minimum pressure over the radius is incompatible with the condition of shock free entry for broad blades.

15. Suggestion of a Circulation Distribution Different from the Distribution of Minimum Loss of Kinetic Energy

The above difficulty cannot be overcome by decreasing the chord near the tip because this would increase $\frac{y}{\tau}$. The only way out of the difficulty is to make $\frac{y}{c}$ $\left(\text{or } \frac{y}{\tau}\right)$ tend to zero at the tip but this does imply that the adequate shape must be given up. One obvious possibility is a non-zero chord length at the tip. It has been proved (see Figures 27 and 30) that the best distribution of circulation over a sector blade gives finite downwash derivative at the tip. However, apart from the difficulties at the edge, other considerations favour an alteration of y rather than of c.

The usual blade shape (usual for the best distribution of circulation) is elliptic near the tip and is very broad. Kinner[6] has shown that for the cap of the sphere with zero angle of attack the circulation distribution over span is not elliptic but parabolic. Therefore a circulation distribution which is parabolic near the tip seems reasonable for the usual propeller blade.

Such circulation distributions are not normally used in the lifting line theory because the downwash integral being defined by its principal value has a logarithmic singularity at the tip in this case. It was mentioned before (section 13) that this is no physical singularity but a mere mathematical difficulty of the lifting line theory. A more serious objection against any deviation from the best distribution is the decrease in efficiency. Fortunately as has already been mentioned in section 13, even quite considerable deviations produce only a slight drop in efficiency.

For/

For the case of the hydrofoil in shock free flow it was shown in section 11 that parabolic circulation distribution together with elliptic chord distribution provides constant downwash derivative over span. This should be about the same in the more complicated case of the propeller. The author's suggestion is to introduce a new circulation distribution

$$y = Ax(1 - x^2) \qquad \ldots(70)$$

over a propeller blade having the developed shape

$$\frac{c}{D} = \frac{4}{\pi\sigma_0}\left[\frac{\pi C_T}{4z\int_0^1 y_0 x\,dx}\sqrt{x^2+\lambda^2}\;y_0 + \frac{x^2+\lambda^2}{\lambda^2}0.08(1-x)\right] \qquad \ldots(71)$$

where y_0 is that of Lock's distribution

$$y_0 = x\sqrt{1-x^2} \qquad \ldots(72)$$

Figure 39 shows this new distribution (70), two of the best distributions (65) together with Lock's approximation (72) arranging that each has the same maximum 0.5. Lock's approximation is very close to the best distribution over the outer part of the blade, for the range of λ considered, whereas the new distribution is close to the best distribution over the inner part but differs from it in the outer part in the desired manner. Introducing (72) into (71) gives

$$\frac{c}{D} = \frac{4}{\pi\sigma_0}\left[\frac{4}{z}C_T x\sqrt{1-x^2}\;\sqrt{x^2+\lambda^2} + \frac{x^2+\lambda^2}{\lambda^2}0.08(1-x)\right] \qquad \ldots(73)$$

To get an impression of the effect of the change from best distribution to distribution (70) a comparison is made between the distribution

$$y_1 = \frac{15}{8z}\pi\lambda C_T x(1-x^2)$$

and the Lock distribution

$$y_2 = \frac{4\lambda}{z}C_T x\sqrt{1-x^2}$$

both applied to the blade 73 (see figure 40) for the example

$$C_T = 0.43 \quad \sigma_0 = 0.49 \quad \lambda = 0.4 \quad z = 3$$

Figure/

Figure 41 shows the distribution of the lift coefficient. The lift coefficient increases over the inner part of the blade for the new distribution γ_1, and tends to zero at the tip as $\sqrt{1 - x^2}$. Now the blade shape (73) was derived so that for Lock's distribution the minimum pressure is uniform over the radius but this is no longer so for the new distribution γ_1 for which the pressure drop is 20% greater than for γ_2 over the inner part of the blade. This seems to be a not unreasonable increase (see Figure 42).

Since the new distribution is no longer the best distribution the Goldstein factor is of no use and the calculation of the induced angles of incidence must be derived by some other means, e.g., Multhopp's method[9]. For shock free entry the pitch angle of the chord must equal the induced angle of advance (see equation 66). It has already been pointed out that for best distribution $x \tan (\beta + \alpha_i)$ is a constant so that these chords would form a true helical surface. Figure 43 shows the deviation of $x \tan (\beta + \alpha_i)$ for both distributions γ_1 and γ_2 from the constant optimum value. It is apparent that the distribution γ_1 requires the blade to have a slight twist towards the tip in order to maintain shock free entry.

Figure 44 gives the thrust distribution. The efficiency is

$$\eta_i = 0.792$$

in both cases.

The main point is the camber correction factor for the new distribution. Up to now the calculation has been carried out for the outline Figure 40 and the advance ratio $\mu\lambda = 0.4$ only. Since for the new circulation distribution there is no singularity in the integrand of the first part I_1 (equation 35) this calculation is easier. The final result is given in Figures 45 and 46. Figure 45 proves as expected that the downwash derivative is constant over the outer part of the blade. Figure 46 shows the new correction factor compared with that for the same blade and advance ratio but with best distribution of circulation.

$\frac{dw_d/v}{d\phi}$ being constant the geometrical camber ratio is from (6) and (22)

$$\frac{f_{geom}}{c} = \frac{\lambda}{4(x^2 + \lambda^2)} \frac{c}{D} \frac{dw_d/v}{d\phi} \qquad \ldots(74)$$

tending to zero at the tip as the chord c. Figure 47 shows the geometrical camber ratios for the example. In the inner part of the blade the new camber ratios are much greater than those for best distribution but towards the tip the latter ones tend to infinity.

16. Summary

To delay the onset of surface cavitation as far as possible the suction developed over the blade should be distributed as uniformly as possible. The flow should meet the leading edge with shock free entry so that the lift is produced only by the camber of the profile. The curvature of the streamlines at the mid-chord line of the blade is

calculated/

calculated by a method which was suggested for the first time by Ludwieg. The present paper gives a different derivation for the result given previously by Ludwieg and Ginzel. The downwash derivative is needed in order to determine the section camber ratios which are necessary to produce the desired circulation and thrust distribution. The circulation distribution over the radius remains arbitrary. For best distribution of circulation, i.e., minimum loss of kinetic energy, over two sets of affine blade shapes the numerical calculations were carried out by Ginzel and Strassl and given in the form of a camber correction factor k to be applied to the camber ratios calculated by the usual lifting line theory of the propeller. For convenience these numerical results are reproduced again here in the form of graphs.

In the second part of the paper the influence on the camber correction factor of blade shape, of number of blades, and of circulation distribution over the radius are shown. Assuming a normal distribution of maximum thickness over a blade the condition of constant minimum pressure over the radius determines an adequate shape of the blade which depends on the circulation distribution. However, the section camber ratio tends to infinity at the tip for these adequate blade shapes, in particular for best distribution over the usual blade shapes which are elliptic in form near the tip. From an exact theory of the lifting surface of the cap of a sphere at zero angle of attack it is known that the circulation distribution over span is parabolic rather than elliptic. It is shown in this paper that for shock free condition and parabolic circulation distribution the downwash derivative is constant along the span.

It is suggested therefore that the best distribution of circulation over a broad propeller blade be replaced by a somewhat altered distribution which is parabolic towards the tip of the blade but the usual blade shape (adequate for best distribution) be retained. The downwash derivative is then constant over the main part of the radius and the camber correction factor is finite and non zero at the tip. The change from best distribution to the new distribution does not affect the efficiency.

References

No.	Author(s)	Title, etc.
1	I. Ginzel and H. Ludwieg	On the theory of the broad bladed propeller. U.M. 3097. A.R.C. 11,067. 1944.
2	H. Strassl	Camber correction for screw propellers. M.A.P. Volkenrode, Ref. M.A.P.-V.G.90-T, 1945.
3	Jahnke-Emde	Tables of higher functions.
4	D. Kuchemann	Tables for the stream function and the velocity components of a source ring and a vortex ring. Jahrbuch 1940 der deutschen Luftfahrtforschung 1, p. 547. A.R.C. 10,615.
5	H. B. Helmbold	On the influence of the contraction of the slipstream on broad bladed propellers. WRH XIV, 1933, p. 319.

No.	Author(s)	Title, etc.
6	W. Kunner	Potential theory of the circular wing. Ing. Arch 8. A.R.C. 8382. 1937.
7	K. Krienes	Potential theory of the elliptic wing. ZAMM 20. A.R.C. 8472. 1940.
8	I. Ginzel	The cap of a sphere and the cap of an ellipsoid of revolution as surfaces of constant downwash derivative. A.R.L. Report A.R.L./R2/G/AE/2/5.
9	H. Multhopp	Digest for the aircraft designer (unpublished) 1947.

Table/

Table of the $K(\chi, \sigma_{\bar{x}})$

$\sigma_{\bar{x}}$ \ χ	89°	87°	85°	80°	75°	70°	65°	60°
0.3	0.06	0.20	0.34	0.68	1.00	1.28	1.53	1.76
0.4	0.08	0.27	0.46	0.91	1.30	1.62	1.89	2.14
0.5	0.16	0.43	0.69	1.28	1.74	2.11	2.39	2.62
0.6	0.24	0.72	1.08	1.88	2.42	2.83	3.09	3.30
0.7	0.42	1.15	1.78	2.90	3.51	3.88	4.14	4.36
0.8	0.82	2.37	3.45	4.90	5.50	5.82	6.03	6.21
0.9	3.24	7.5	9.22	10.6	11.0	11.30	11.46	11.58
1.0	∞	∞	∞	∞	∞	∞	∞	∞
1.1	-3.28	-6.9	-8.1	-8.7	-8.7	-8.64	-8.57	-8.50
1.2	-0.86	-2.25	-3.05	-3.80	-3.93	-3.91	-3.89	-3.86
1.4	-0.22	-0.62	-0.96	-1.47	-1.62	-1.67	-1.66	-1.65
1.6	-0.12	-0.30	-0.47	-0.75	-0.90	-0.96	-0.98	-0.98
1.8	-0.05	-0.16	-0.26	-0.45	-0.56	-0.62	-0.64	-0.65
2.0	-0.03	-0.10	-0.17	-0.30	-0.39	-0.44	-0.46	-0.47
2.4	-0.02	-0.05	-0.08	-0.16	-0.21	-0.26	-0.27	-0.28
3.0	-0.01	-0.03	-0.05	-0.08	-0.11	-0.14	-0.15	-0.16
3.6	0	-0.02	-0.03	-0.05	-0.07	-0.08	-0.09	-0.10
4.2	0	-0.01	-0.02	-0.03	-0.05	-0.06	-0.06	-0.07
4.6	0	0	-0.01	-0.02	-0.04	-0.04	-0.05	-0.05

Table of the $K(\chi, \sigma_{\bar{x}})$. Surroundings of $\sigma_{\bar{x}} = 1$

$\sigma_{\bar{x}}$ \ χ	89°	87°	85°	80°	75°	70°	65°	60°
0.9	3.24	7.50	9.22	10.6	11.0	11.3	11.5	11.6
0.95	11.5	18.7	20.1	21.1	21.4	21.7	21.8	21.9
0.97	25.8	33.0	34.0	34.8	35.1	35.3	35.4	35.5
0.98	44.3	50.2	51.1	51.7	52.0	52.1	52.3	52.4
0.99	96.8	101.0	101.4	102.1	102.3	102.5	102.6	102.7
1.0	∞	∞	∞	∞	∞	∞	∞	∞
1.01	-94.8	-98.0	-97.8	-97.8	-97.7	-97.5	-97.4	-97.3
1.02	-42.9	-47.9	-48.2	-48.1	-48.0	-47.9	-47.8	-47.7
1.03	-25.0	-31.0	-31.6	-31.7	-31.5	-31.4	-31.3	-31.2
1.05	-11.4	-17.3	-18.2	-18.5	-18.4	-18.3	-18.2	-18.2
1.10	-3.28	-6.9	-8.1	-8.7	-8.7	-8.64	-8.57	-8.50

ADDENDUM/

Influence of the Other Blades on the Propeller Blade Camber Factor

ADDENDUM

Abstract

The exact expression is derived for the downwash derivative at the mid-chord line of a propeller blade produced by the vortex surfaces of the second and third blades of a three-bladed propeller. The influence of these blades is to reduce the curvature of flow induced by the vortex surface of the original blade. The effect on the camber correction factor is given as an influence factor i in Figure 48 which has been derived for one particular blade shape and another of half the width with several circulation distributions and one ratio of advance. For best distribution of circulation and usual blade shapes the factor might be applied generally.

1. Introduction

The numerical values of the camber factor given in previous reports[1] are based on the downwash derivative produced by the vortex system of the original blade only, because the influence of the other blades was presumed to be negligibly small. This supposition was based on the results of an approximate method in which the remaining blades were replaced by sector blades of the same blade area as the original one with constant radial circulation distribution, each blade giving the same thrust as the original blade.

Since it is rather difficult to judge the validity of the approximation it seemed desirable to derive the exact solution and calculate a few examples. The equations can be derived according to the method used in sections 5 and 6 of reference 1 and split up in two parts accordingly. Although they refer to a three bladed propeller, this is no fundamental restriction since by inserting other angles instead of $\frac{2\pi}{3}$ and $\frac{4\pi}{3}$ in the equations any possible arrangement may be covered.

2. First Part of the Downwash Derivative

The first part of the downwash derivative is that produced by the g_r vortices of the second blade and the g_ϕ vortices of strength given by the second term of (21) in reference 1. [The starred numbers of the equations and figures correspond to those unstarred in reference 1.] The pivotal point is $x = x^*$, $\phi = \phi^*$ (see Figure 8*) and the points of the second blade have co-ordinates x and $\frac{2\pi}{3} + \phi, \phi$ varying from $-\frac{\bar{\tau}}{2}(x)$ to $\frac{\bar{\tau}}{2}(x)$.

The radius NQ in the second blade has direction cosines

$$\cos \mu_1 = \cos\left(\phi^* - \frac{2\pi}{3} - \phi\right)$$

$$\cos \nu_1 = \sin\left(\phi^* - \frac{2\pi}{3} - \phi\right) \qquad \ldots(26^*)$$

$$\cos \tau_1 = 0$$

and/

and PQ has direction cosines

$$\cos \mu_2 = \frac{x \cos\left(\phi^* - \frac{2\pi}{3} - \phi\right) - x^*}{a}$$

$$\cos \nu_2 = \frac{x \sin\left(\phi^* - \frac{2\pi}{3} - \phi\right)}{a} \qquad \ldots(27^*)$$

$$\cos \tau_2 = \frac{\lambda\,(\phi^* - \phi)}{a}$$

and a itself

$$\frac{a^2}{R^2} = x^2 + x^{*2} - 2xx^* \cos\left(\frac{2\pi}{3} + \phi - \phi^*\right) + \lambda^2\,(\phi^* - \phi)^2 \qquad \ldots(28^*)$$

Therefore the whole system of radial vortices of the second blade gives from (31) in reference 1 the downwash component

$$\frac{1}{2\pi}\int_0^1 \int_{-\frac{\tau}{2}}^{\frac{\tau}{2}} \frac{\gamma}{\tau} \frac{-\lambda^2(\phi - \phi^*)\cos\left(\frac{2\pi}{3} + \phi - \phi^*\right) - x^{*2}\sin\left(\frac{2\pi}{3} + \phi - \phi^*\right)}{\left[x^2 + x^{*2} - 2xx^*\cos\left(\frac{2\pi}{3} + \phi - \phi^*\right) + \lambda^2(\phi - \phi^*)^2\right]^{3/2}\sqrt{x^{*2} + \lambda^2}} d\phi dx \qquad \ldots(31^*)$$

where $\gamma = \frac{\Gamma}{vD}$. $\qquad \ldots(32^*)$

The second term of (21) in reference 1 gives correspondingly

$$-\frac{1}{2\pi}\Big/$$

$$-\frac{1}{2\pi}\int_0^1\int_{-\frac{\bar{\tau}}{2}}^{\frac{\bar{\tau}}{2}}\frac{\gamma\bar{\tau}'}{2\bar{\tau}}\frac{-\lambda^2\left\{x\cos\left(\frac{2\pi}{3}+\phi-\phi^*\right)-x^*+x(\phi-\phi^*)\sin\left(\frac{2\pi}{3}+\phi-\phi^*\right)\right\}-xx^*\left\{x-x^*\cos\left(\frac{2\pi}{3}+\phi-\phi^*\right)\right\}}{\left[x^2+x^{*2}-2xx^*\cos\left(\frac{2\pi}{2}+\phi-\phi^*\right)+\lambda^2(\phi-\phi^*)^2\right]^{3/2}\sqrt{x^{*2}+\lambda^2}}\,d\phi dx \quad \ldots(34^*)$$

Now add (31*) to (34*). For the influence of the third blade the same expression holds with $\frac{4\pi}{3}$ replacing $\frac{2\pi}{3}$.

For the downwash derivative in chordwise direction the expression must be differentiated with respect to ϕ^*. Since ϕ and ϕ^* occur in the combination $\phi - \phi^*$ only the differentiation with respect to ϕ^* and the integration with respect to ϕ can be accomplished by omitting the ϕ integral and replacing ϕ by its limits $\frac{\bar{\tau}}{2}$ and $-\frac{\bar{\tau}}{2}$ and introducing a negative sign. For the part (31*) the difference between the upper and lower limits is taken since the remaining radial vorticity at the leading edge and that at the trailing edge are of opposite sign when taking the difference between the original vortex surface and the one moved in chord direction.

For the part (34*) special consideration is necessary. As can be seen from equation (16) in reference 1 there is the term $-\frac{\Gamma\bar{\tau}'}{2\tau}$ which is the initial value of the helical vortices at the leading edge being the helical wise component of the circumferential vortex. At the trailing edge another term $-\frac{\Gamma\bar{c}'}{2\bar{c}}$ or $-\frac{\Gamma\bar{\tau}'}{2\tau}$ must be added (see Figure 4 in reference 1). This can be interpreted either as the part of the circumferential vortex in helical direction or as that part of the trailing vortices which does not cancel out when the difference is taken between the original vortex surface and the one moved in chord direction. The two remainder infinitesimal vortex pieces are of the same sign. Consequently the two limits for the part (34*) have to be added.

This consideration applied in the derivation of equation (35) in reference 1 as well but was not mentioned since the symmetry of the whole effect was obvious.

In/

In the present case of (31*) and (34*), however, the integrand shows no symmetry with $\phi^* = 0$. Then the downwash derivative

$$\frac{d_{wd_1}/v}{d\phi} = \frac{1}{2\pi}\int_0^1 \frac{y}{\bar{\tau}} \frac{\lambda^2 \frac{\bar{\tau}}{2}\cos\left(\frac{2\pi}{3}-\frac{\bar{\tau}}{2}\right) - x^{*2}\sin\left(\frac{2\pi}{3}-\frac{\bar{\tau}}{2}\right) + \frac{\bar{\tau}'}{2}\left[-\lambda^2\left\{x\cos\left(\frac{2\pi}{3}-\frac{\bar{\tau}}{2}\right) - x\frac{\bar{\tau}}{2}\sin\left(\frac{2\pi}{3}-\frac{\bar{\tau}}{2}\right) - x^*\right\} - xx^*\left\{x - x^*\cos\left(\frac{2\pi}{3}-\frac{\bar{\tau}}{2}\right)\right\}\right]}{\sqrt{x^{*2}+\lambda^2}\left[x^2 + x^{*2} - 2xx^*\cos\left(\frac{2\pi}{3}-\frac{\bar{\tau}}{2}\right) + \lambda^2\left(\frac{\bar{\tau}}{2}\right)^2\right]^{3/2}} dx$$

$$+ \frac{1}{2\pi}\int_0^1 \frac{y}{\bar{\tau}} \frac{\lambda^2 \frac{\bar{\tau}}{2}\cos\left(\frac{2\pi}{3}+\frac{\bar{\tau}}{2}\right) + x^{*2}\sin\left(\frac{2\pi}{3}+\frac{\bar{\tau}}{2}\right) + \frac{\bar{\tau}'}{2}\left[-\lambda^2\left\{x\cos\left(\frac{2\pi}{3}+\frac{\bar{\tau}}{2}\right) + x\frac{\bar{\tau}}{2}\sin\left(\frac{2\pi}{3}+\frac{\bar{\tau}}{2}\right) - x^*\right\} - xx^*\left\{x - x^*\cos\left(\frac{2\pi}{3}+\frac{\bar{\tau}}{2}\right)\right\}\right]}{\sqrt{x^{*2}+\lambda^2}\left[x^2 + x^{*2} - 2xx^*\cos\left(\frac{2\pi}{3}+\frac{\bar{\tau}}{2}\right) + \lambda^2\left(\frac{\bar{\tau}}{2}\right)^2\right]^{3/2}} dx \quad (4)$$

A check on the equation is obtained by replacing $\frac{2\pi}{3}$ by 0; then this expression reduces to (35) of reference 1.

For convenience the angles should be expressed by those in the first quadrant. Then

$$\frac{dw_1/v}{d\phi} = \frac{1}{2\pi}\int_0^1 \frac{y}{\bar{\tau}} \frac{-\lambda^2 \frac{\bar{\tau}}{2}\cos\left(\frac{\pi}{3}+\frac{\bar{\tau}}{2}\right) - x^{*2}\sin\left(\frac{\pi}{3}+\frac{\bar{\tau}}{2}\right) + \frac{\bar{\tau}'}{2}\left[\lambda^2\left\{x\cos\left(\frac{\pi}{3}+\frac{\bar{\tau}}{2}\right) + x\frac{\bar{\tau}}{2}\sin\left(\frac{\pi}{3}+\frac{\bar{\tau}}{2}\right) + x^*\right\} - xx^*\left\{x + x^*\cos\left(\frac{\pi}{3}+\frac{\bar{\tau}}{2}\right)\right\}\right]}{\sqrt{x^{*2}+\lambda^2}\left[x^2 + x^{*2} + 2xx^*\cos\left(\frac{\pi}{3}+\frac{\bar{\tau}}{2}\right) + \lambda^2\left(\frac{\bar{\tau}}{2}\right)^2\right]^{3/2}} dx$$

$$+ \frac{1}{2\pi}\int \frac{y}{\bar{\tau}} \frac{-\lambda^2 \frac{\bar{\tau}}{2}\cos\left(\frac{\pi}{3}-\frac{\bar{\tau}}{2}\right) + x^{*2}\sin\left(\frac{\pi}{3}-\frac{\bar{\tau}}{2}\right) + \frac{\bar{\tau}'}{2}\left[\lambda^2\left\{x\cos\left(\frac{\pi}{3}-\frac{\bar{\tau}}{2}\right) - x\frac{\bar{\tau}}{2}\sin\left(\frac{\pi}{3}-\frac{\bar{\tau}}{2}\right) + x^*\right\} - xx^*\left\{x + x^*\cos\left(\frac{\pi}{3}-\frac{\bar{\tau}}{2}\right)\right\}\right]}{\sqrt{x^{*2}+\lambda^2}\left[x^2 + x^{*2} + 2xx^*\cos\left(\frac{\pi}{3}-\frac{\bar{\tau}}{2}\right) + \lambda^2\left(\frac{\bar{\tau}}{2}\right)^{2-3/2}\right]} dx \qquad \ldots(35^*)$$

Inserting $\frac{4\pi}{3}$ instead of $\frac{2\pi}{3}$ in the above equation and then expressing by the angles in the first quadrant the result is the same but the two integrals appear in the reverse order. Therefore the first part of the downwash derivative produced by both blades is

$$\frac{dw_1/v}{d\phi} = I_1 = \frac{1}{\pi}\int_0^1 J_{11}\,dx + \frac{1}{\pi}\int_0^1 J_{12}\,dx = \frac{1}{\pi}\int_0^1 J_1\,dx \qquad \ldots(35^{**})$$

Again/

Again (see section 9 in reference 1) the integrand J_1 of (35**) tends to infinity at the tip as $\frac{1}{\sqrt{1-x}} = \frac{1}{u}$ for best distribution and usual blade shapes. The same process as suggested in the previous report can be used, this time the limiting value $2uJ_1$ at $u = 0$ has the value

$$\sqrt{\frac{3}{\lambda}}\,\frac{2}{(1+\lambda^2)^{3/4}}\,\frac{\lambda^2\left(\frac{1}{2}+x^*\right)-x^*\left(1+\frac{x^*}{2}\right)}{\sqrt{\lambda^2+x^{*2}}\,(1+x^{*2}+x^*)^{3/2}}$$

or

$$\lim\left(\frac{\Gamma}{u}\right)2\,\frac{\lambda^2\left(\frac{1}{2}+x^*\right)-x^*\left(1+\frac{x^*}{2}\right)}{\sqrt{\lambda^2+x^{*2}}\,(1+x^{*2}+x^*)^{3/2}}$$

for any other distribution tending to zero at the tip as $\sqrt{1-x}$.

4. Second Part of the Downwash Derivative

The velocity induced at point P by the term

$$-\frac{d}{dx}\left(\frac{\Gamma}{\tau}\right)\phi \qquad -\frac{\bar{\tau}}{2} \leq \phi \leq \frac{\bar{\tau}}{2}$$

of the helical vortices g_ϕ can be written as

$$\frac{w_{d_2}}{v} = -\frac{1}{2\pi}\int_0^1\int_{-\frac{\bar{\tau}}{2}}^{\frac{\bar{\tau}}{2}} \frac{\cos\theta}{\bar{x}}\,\frac{d}{dx}\left(\frac{\gamma}{\tau}\right)\phi\,\frac{dK\left(\frac{2\pi}{3}+\phi-\phi^*,\,x,\,x^*\right)}{d\phi}\,d\phi dx \qquad \ldots(36^*)$$

with a slight modification to (36) introducing immediately the kernel K which is actually built up not from helical vortices of radius x but from circular arcs of radius 1. This is the same as in reference 1.

Partial integration with respect to ϕ gives

$$-\frac{1}{2\pi}\int_0^1 \frac{\cos\theta}{\bar{x}}\,\frac{d}{dx}\left(\frac{\gamma}{\tau}\right)\left[\phi\int\frac{dK}{d\phi}\left(\frac{2\pi}{3}+\phi-\phi^*,\,x,\,x^*\right)d\phi\right]_{-\frac{\bar{\tau}}{2}}^{\frac{\bar{\tau}}{2}} +$$

$$+\frac{1}{2\pi}\int_0^1\int_{-\frac{\bar{\tau}}{2}}^{\frac{\bar{\tau}}{2}} \frac{\cos\theta}{\bar{x}}\,\frac{d}{dx}\left(\frac{\gamma}{\tau}\right)K\left(\frac{2\pi}{3}+\phi-\phi^*\right)d\phi dx$$

Again/

Again ϕ and ϕ^* occur in the combination $\phi - \phi^*$ only. This means integration with respect to ϕ and differentiation with respect to ϕ^* cancel each other and ϕ may straight away be repaced by the limits $\frac{\bar{\tau}}{2}$ and $-\frac{\bar{\tau}}{2}$; and ϕ^* is put zero. The first term does not vanish since it is no longer symmetrical. The third blade gives the same contribution; the integrand between $-\frac{\bar{\tau}}{2}$ and 0 of the second blade equals that between 0 and $\frac{\bar{\tau}}{2}$ of the third blade. Then the downwash derivative becomes

$$\frac{d_{wd_2}/v}{d\phi} = I_2 = \frac{1}{\pi}\int \frac{\cos\theta}{\bar{x}} \frac{d}{dx}\left(\frac{\gamma}{\bar{\tau}}\right)\left[\frac{\bar{\tau}}{2}\frac{dK}{d\phi}\left(\frac{\bar{\tau}}{2}\right) - K\left(\frac{\bar{\tau}}{2},x,x^*\right) - \frac{\bar{\tau}}{2}\frac{dK}{d\phi}\left(-\frac{\bar{\tau}}{2}\right) + K\left(-\frac{\bar{\tau}}{2},x,x^*\right)\right] dx \quad \ldots(44^*)$$

with

$$\theta = \arctan\frac{\lambda}{x} - \arctan\frac{\lambda}{x^*} \quad \ldots(45^*)$$

K is the velocity induced by a vortex of unit strength and of circular arc form between $\frac{2\pi}{3} - \frac{\bar{\tau}}{2}$ and $\frac{2\pi}{3} + \frac{\bar{\tau}}{2}$ and of radius 1. Since the replacing circular arc is to pass through the mid-point of the helical arc its centre lies beyond the axis at distance $\bar{x} - x$. The distance of the pivotal point P to the centre of the circular arc is therefore given by (see Figure 10*)

$$\sigma_{\bar{x}} = \frac{\sqrt{x^{*2} + (\bar{x}-x)^2 + 2x^*(\bar{x}-x)\cos\frac{2\pi}{3}}}{\bar{x}} = \frac{\sqrt{x^{*2} + (\bar{x}-x)^2 - x^*(\bar{x}-x)}}{\bar{x}} \quad \ldots(39^*)$$

Biot-Savarts' law gives the induced velocity

$$K = \int_{-\frac{\bar{\tau}}{2}}^{\frac{\bar{\tau}}{2}} \frac{1 - \sigma_{\bar{x}}\cos\left(\frac{2\pi}{3} - \phi'\right)}{\left[1 + \sigma_{\bar{x}}^2 - 2\sigma_{\bar{x}}\cos\left(\frac{2\pi}{3} - \phi'\right)\right]^{3/2}} d\phi' = \int_{-\frac{\bar{\tau}}{2}}^{\frac{\bar{\tau}}{2}} \frac{1 + \sigma_{\bar{x}}\cos\left(\frac{\pi}{3} + \phi'\right)}{1 + \sigma_{\bar{x}}^2 + 2\sigma_{\bar{x}}\cos\left(\frac{\pi}{3} + \phi'\right)^{3/2}} d\phi'$$

5./

5. The Numerical Results

Since it is convenient for the calculation to use a blade shape given by an analytical expression the shape Figure 40 (reference 1) was used which is very similar to the 100% blade of shape 1 (Figure 13 in reference 1). There is a slight deviation from shape 1 over the inner part up to 0.7, where the blade Figure 40 is straighter (similar to shape 2, Figure 14 in reference 1). This results in a slight deviation of the uncorrected camber factors from those given for shape 1.

For this shape and the affine one of half the width (50%) of the original (100%) the expressions (35**) and (44*) have been calculated The result is plotted in figure 48 in the form of a correction i where

$$\left(\frac{1}{k}\right)_{corr.} = \left(\frac{1}{k}\right)_{uncorr.} (1 - i) \qquad \ldots(75)$$

and $k_{uncorr.}$ is the camber factor as given in previous reports so giving the new corrected one $k_{corr.}$.

This factor i is given for best distribution with $\lambda = 0.4$. It depends on the blade shape and largely on the circulation distribution. Look's distribution $\Gamma = x\sqrt{1 - x^2}$ deviates from the best distribution for $\lambda = 0.4$ mainly over the inner part. Hence the difference in i (and in k) for the inner parts of the blade (see dashed curve in Figure 48). The corrected and uncorrected camber factors for best distribution can be seen in Figure 49.

The influence of the other blades decreases the curvature effect of the original one especially over the inner part of the blade. This is mainly due to the helical vortices covering the blade since the kernel function does no longer change sign along the radius because the pivotal point is outside the blade. Since such vortices near the axis would give an unreasonably large contribution, the calculation has been made with the part from 0 to 0.2 of the integral (44*) omitted. Even then for the wide blade the part (44*) was 14 times the part (35**) at $x = 0.3$, 4.5 times at $x = 0.5$, and 3 times at $x = 0.7$. For the 50% blade the part (44*) was 2 times that of 35** at $x = 0.3$ and at $x = 0.5$, and about the same at $x = 0.7$. For the contributions from the original blade, the part I_1 is always much greater than I_2.

This effect of the positive kernel function is overwhelming for circulation distributions with positive $\frac{d}{dx}\left(\frac{\gamma}{\tau}\right)$ over the radius as for instance the best distribution over outlines like shape 1 (see section 13 in reference 1). For the new distribution $\gamma = x(1 - x^2)$ suggested in reference 1 conditions are different. Then $\frac{d}{dx}\left(\frac{\gamma}{\tau}\right)$ changes sign over radius and the contribution (44*) of the "cascade effect" becomes very small. Then the increase in k as indicated in Figure 50 is almost solely due to the circumferential vortices of the other blades. That this would result in a reduced downwash derivative was already pointed out in section 7 of reference 1. The correction i is very small and nearly constant along the blade (see Figure 48).

6./

6. Summary

The exact solution for the influence of the remaining blades on the curvature of flow at the centre line ofmthe initial blade has shown that for usual blade shapes with circulation distributions near the optimum this "cascade effect" on the camber correction always increases the k factor tending to counteract the influence of the original blade. For best distribution of circulation the effect on the sections near the root is greater than expected from approximate calculations, being an increase of up to 10% on the k factor for very broad three bladed propellers. The effect decreases rapidly towards the tip as shown in Figure 48. The influence factor i given in this Figure may be applied to all camber factors previously published which refer to best distribution and usual shapes. For the new circulation distribution suggested in the previous report the "cascade influence" is small over all the blade as shown in Figure 48 and Figure 50. It should again be noted that the camber factor (and the cascade influence on it) are of doubtful validity at sections near the axis since the hub is not properly allowed for.

Reference

No.	Author(s)	Title, etc.
1	I. Ginzel	Theory of the broad-bladed propeller. A.R.L. Report. A.R.L./R3/G/HY/7/1. A.R.C. 15,120. (See forepart of this Report.)

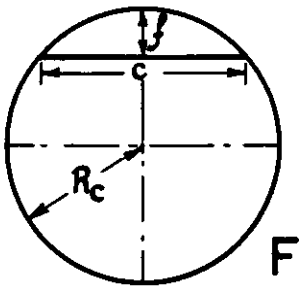

FIG.1

DEFINITION OF THE CAMBER

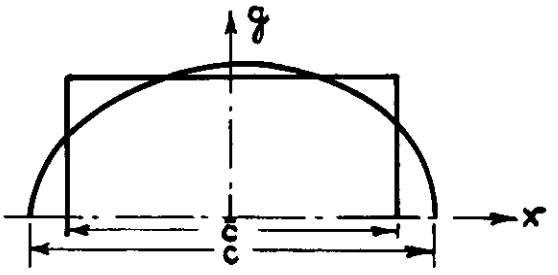

DEFINITION OF THE REDUCED CHORD

FIG.2

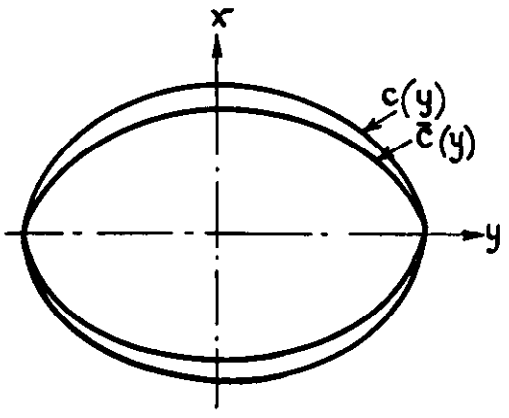

THE REDUCED OUTLINE

FIG.3

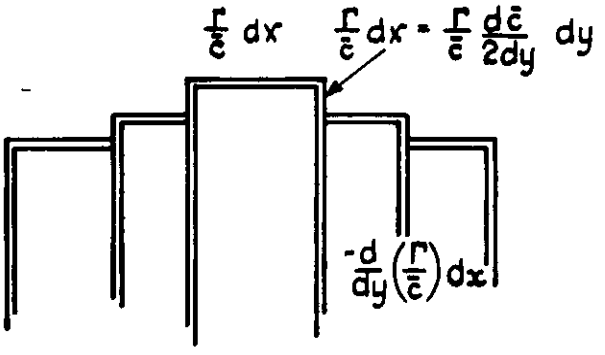

THE CIRCUMFERENTIAL VORTEX (AEROFOIL)

FIG.4

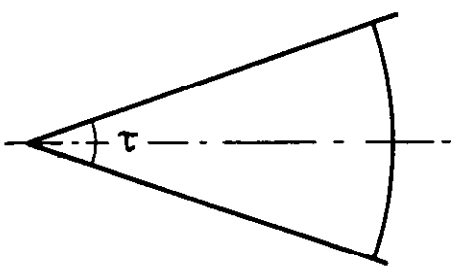

THE SECTOR BLADE

FIG.5

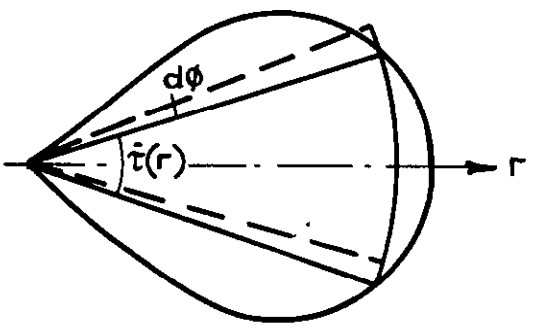

THE ANGLE τ VARIES OVER RADIUS FOR THE USUAL BLADE SHAPE

FIG.6

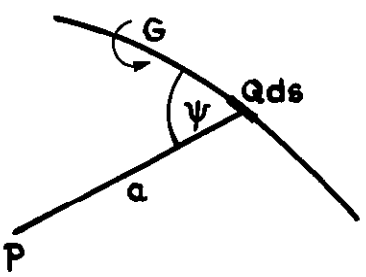

SYMBOLS IN BIOT SAVART'S LAW

FIG.7

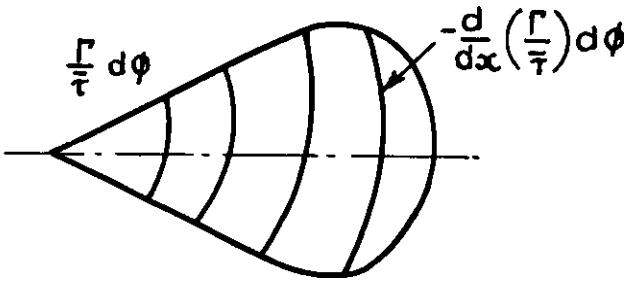

THE REMAINDER VORTEX SYSTEM, PRODUCING THE DOWN-WASH DERIVATIVE

FIG.9

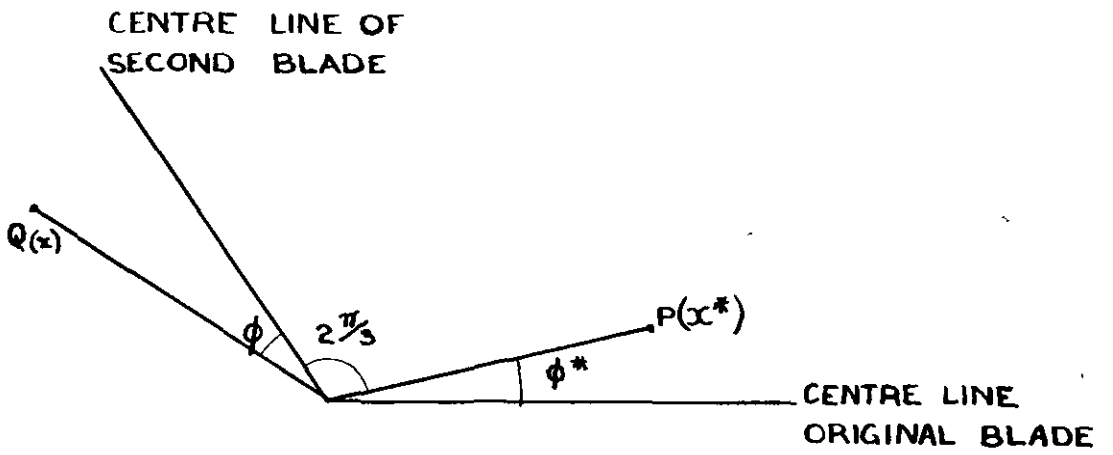

PLAN VIEW. POSITION OF THE PIVOTAL POINT P OFF THE SECOND BLADE.

FIG. 8*

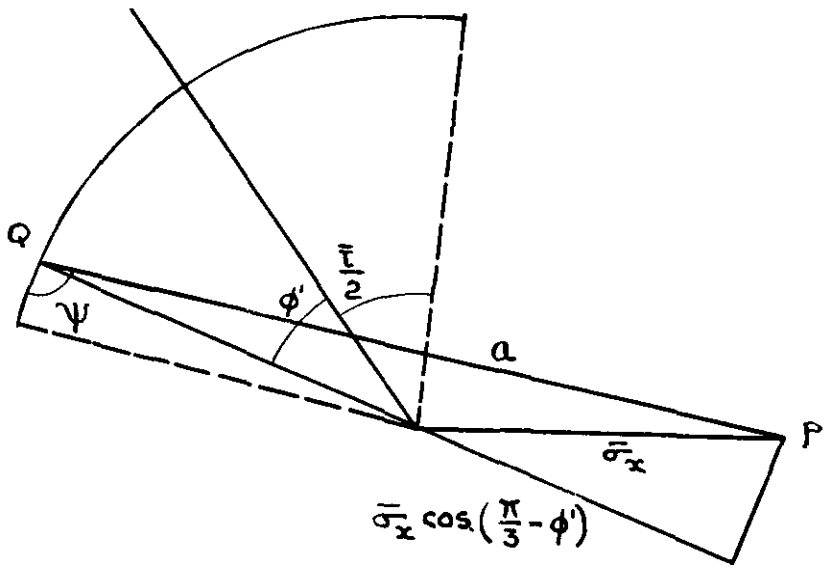

THE "HELICAL" VORTICES OF THE REMAINDER SYSTEM

FIG. 10*

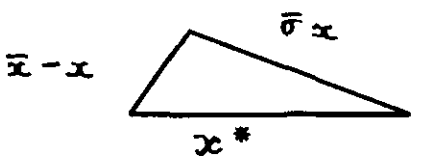

DEFINITION OF $\bar{\sigma}_x$

FIG. 10a

A.R.L./R4/G/HY/7/1

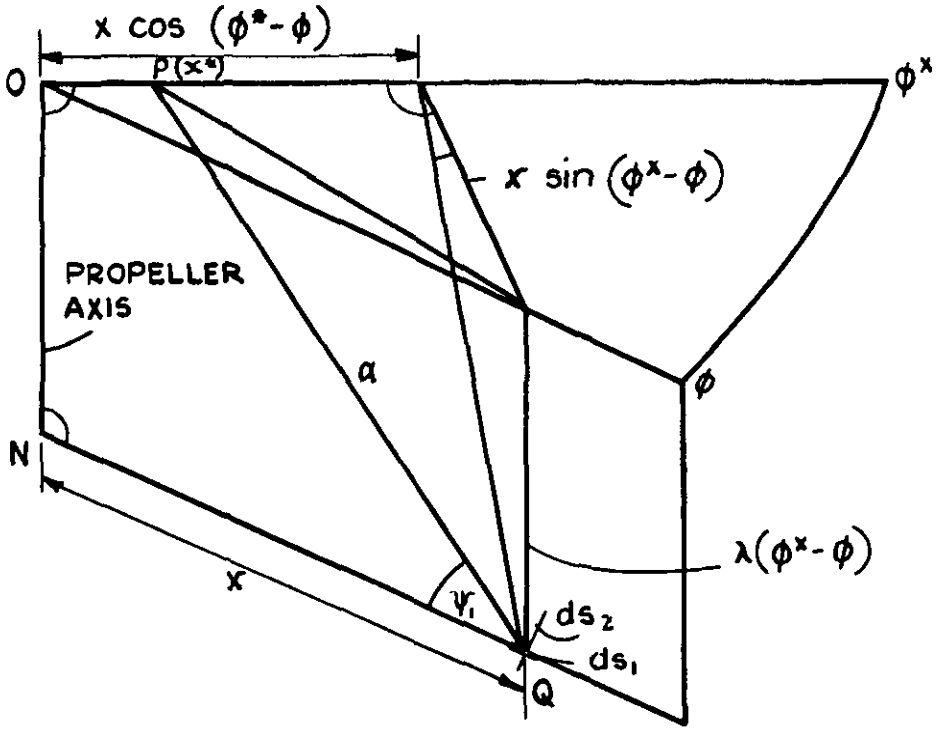

THE VORTEX SYSTEM OF THE PROPELLER BLADE

FIG.8

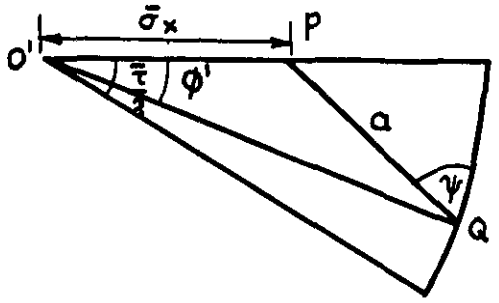

THE HELICAL VORTICES OF THE REMAINDER VORTEX SYSTEM

FIG.10

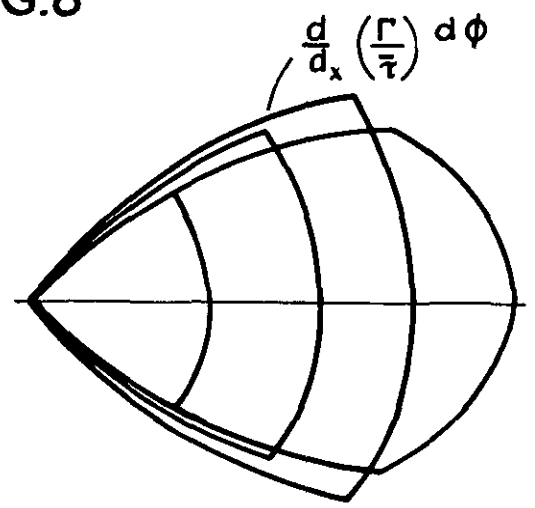

ANOTHER CONCEPTION OF THE REMAINDER VORTEX SYSTEM

FIG.11

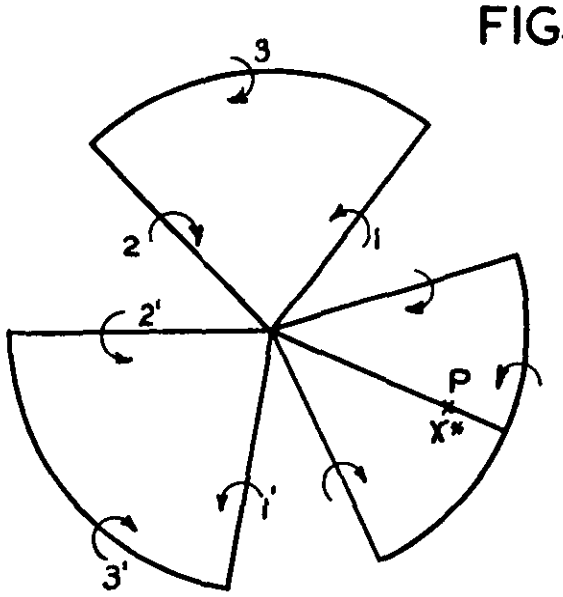

INFLUENCE OF THE SECOND AND THIRD BLADE ON THE DOWNWASH DERIVATIVE

FIG.12

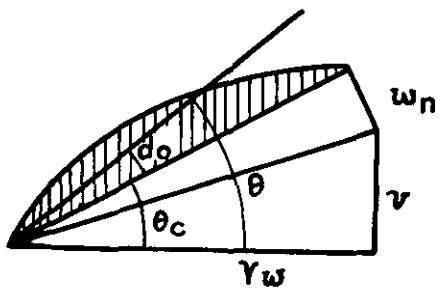

DEFINITION OF THE PITCH ANGLES

FIG. 33

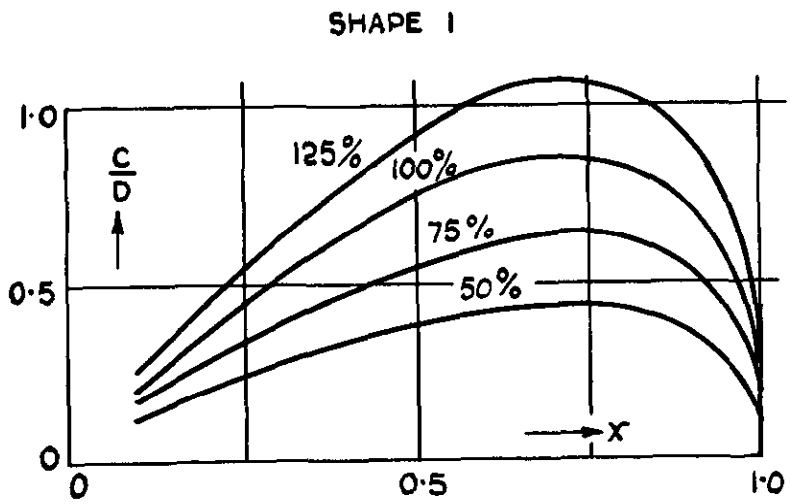

ORIGINAL DEVELOPED BLADE (100%) AND SOME AFFINE BLADE SHAPES CALLED SHAPE 1 IN THIS PAPER

FIG. 13

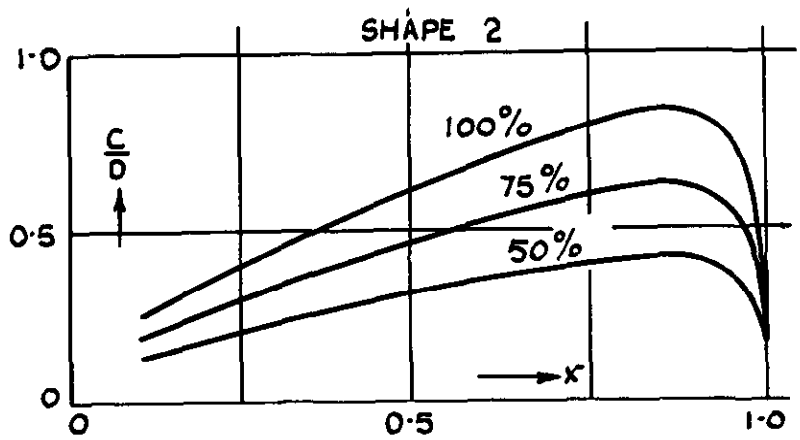

ORIGINAL DEVELOPED BLADE (100%) AND SOME AFFINE BLADE SHAPES CALLED SHAPE 2 IN THIS PAPER

FIG. 14

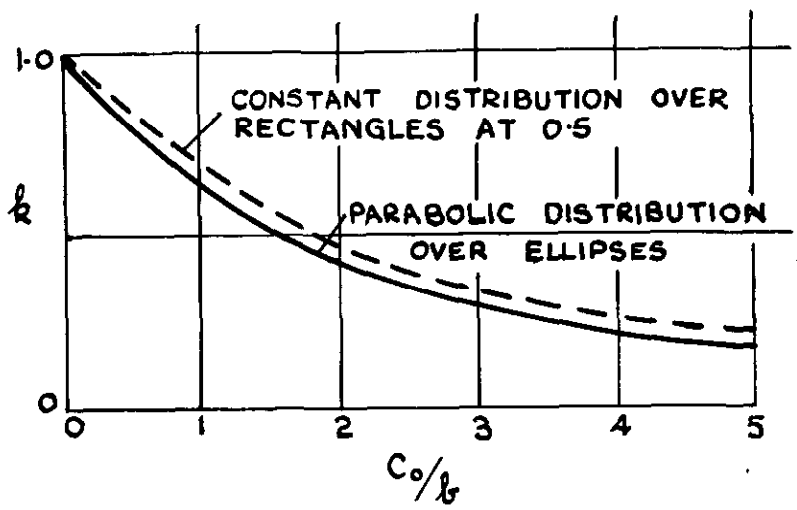

THE CAMBER CORRECTION FACTOR AS A FUNCTION OF THE ASPECT RATIO OF ELLIPTICAL WINGS

FIG. 17

A.R.L/R3/G/HY/7/1

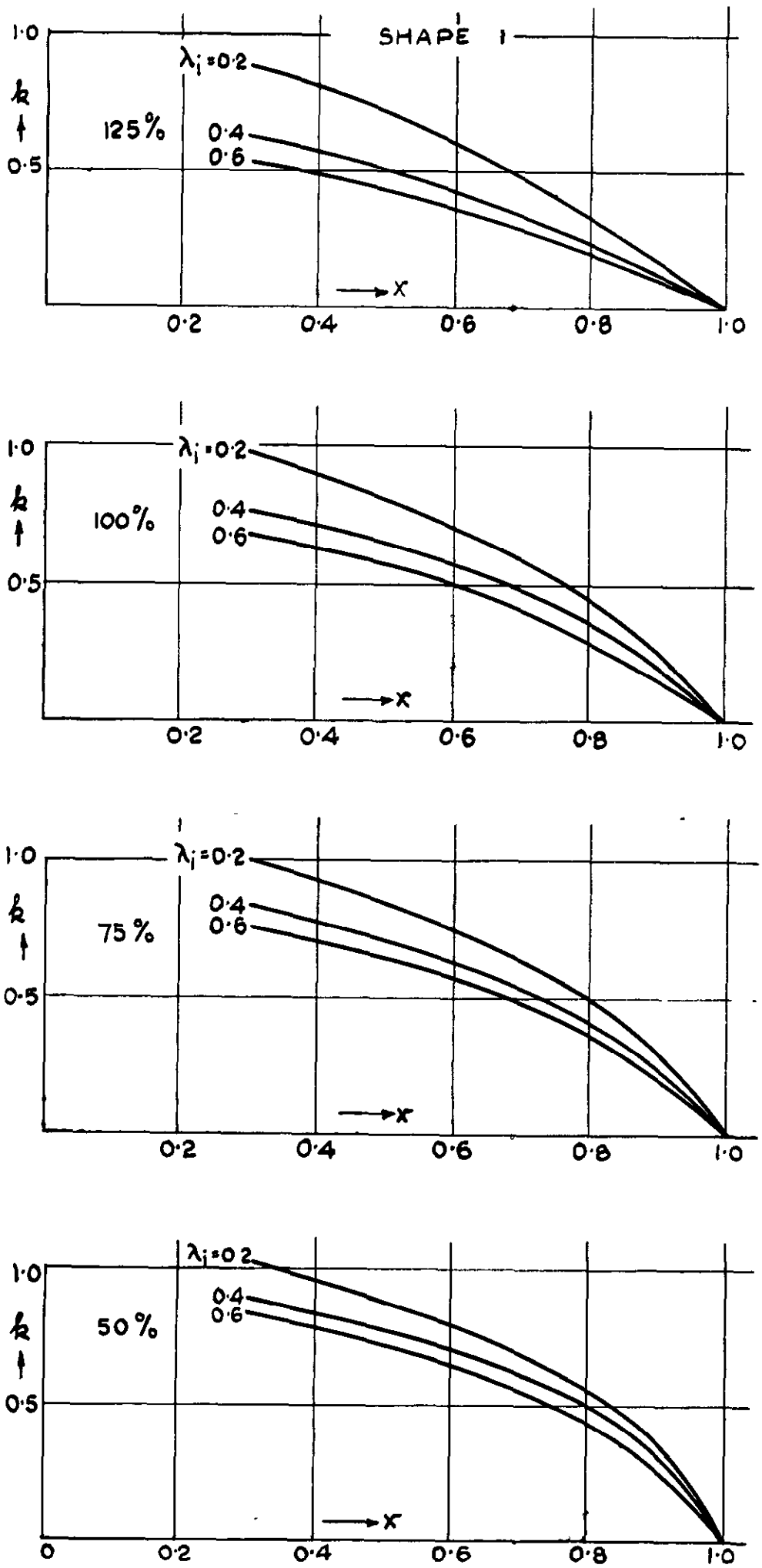

THE CAMBER CORRECTION FACTOR FOR SHAPE 1 (FIG.13)

A.R.L | R3 | G | HY | 7 | 1

FIG.15

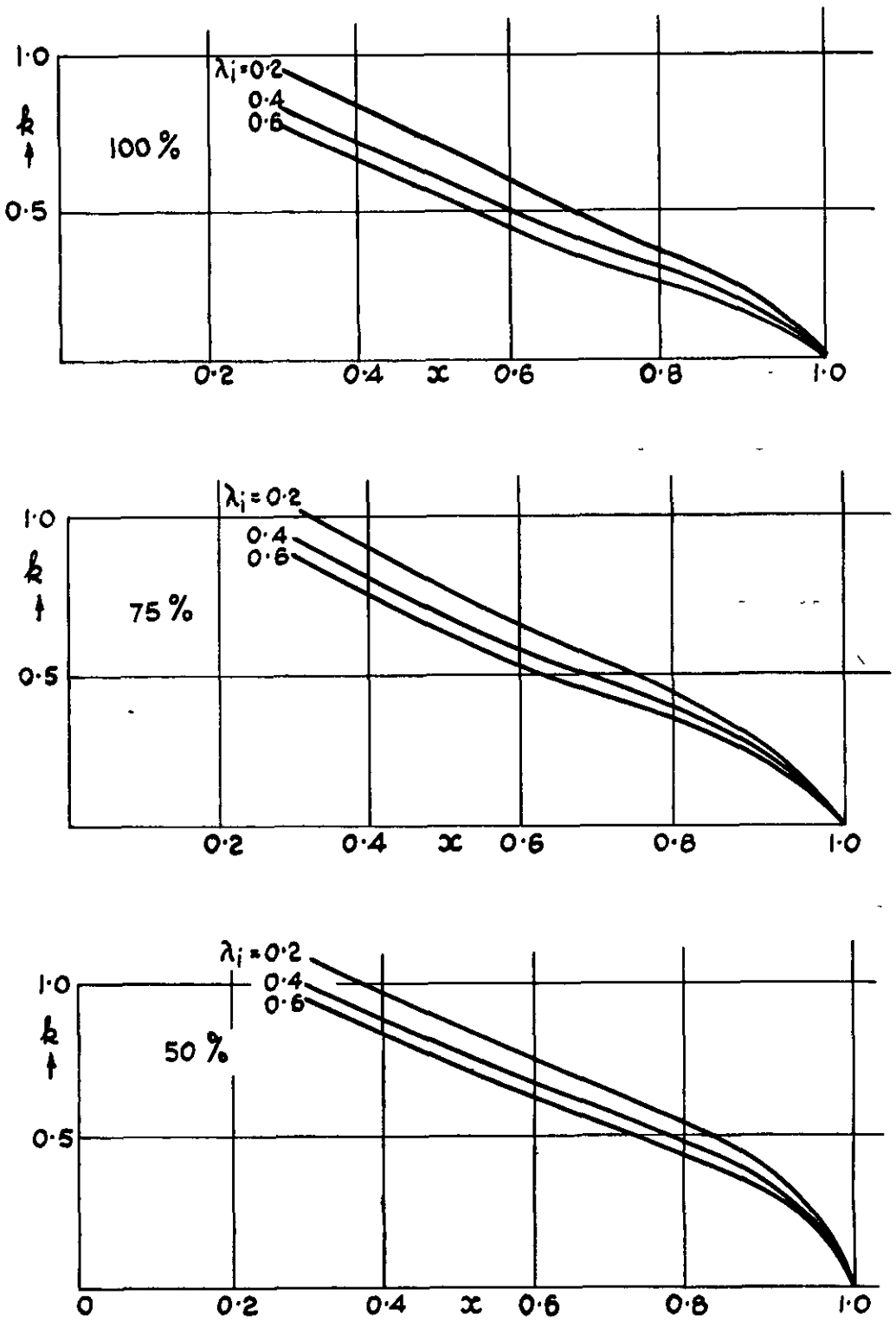

THE CAMBER CORRECTION FACTOR FOR SHAPE 2 (FIG.14)

A.R.L | R3 | G | HY | 7 | 1

FIG.16

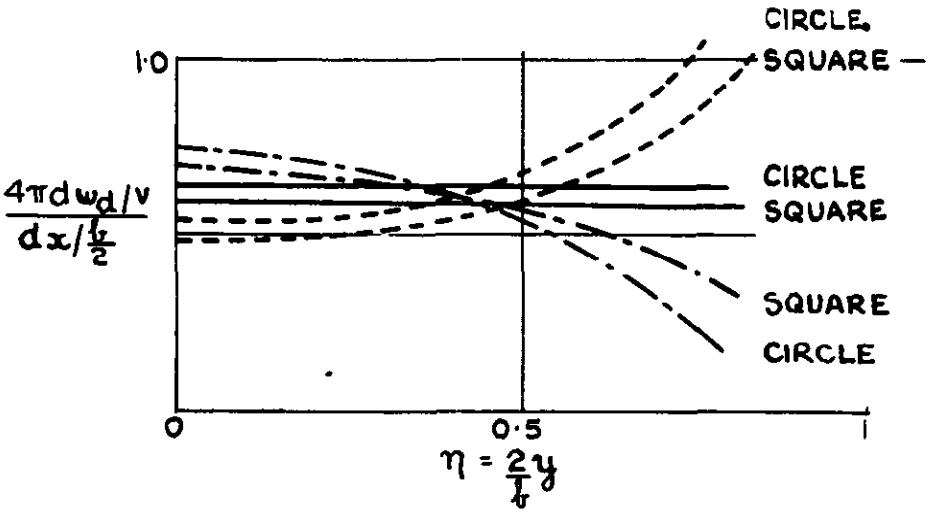

A $A : \frac{\Gamma}{C} = 1$

B $B : \frac{\Gamma}{C} = \sqrt{1-\eta^2}$

C $C : \frac{\Gamma}{C} = 1-\eta^2$

THE DOWNWASH DERIVATIVE AS A FUNCTION OF CIRCULATION / CHORD (AEROFOIL)

FIG. 18

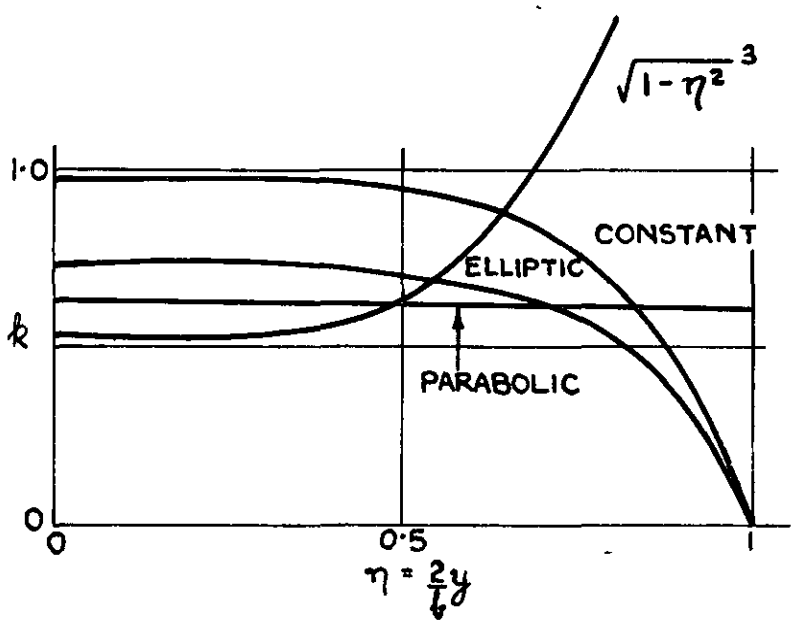

THE INFLUENCE OF CIRCULATION DISTRIBUTION ON THE CAMBER CORRECTION FACTOR OF THE CIRCULAR AEROFOIL.

FIG. 19

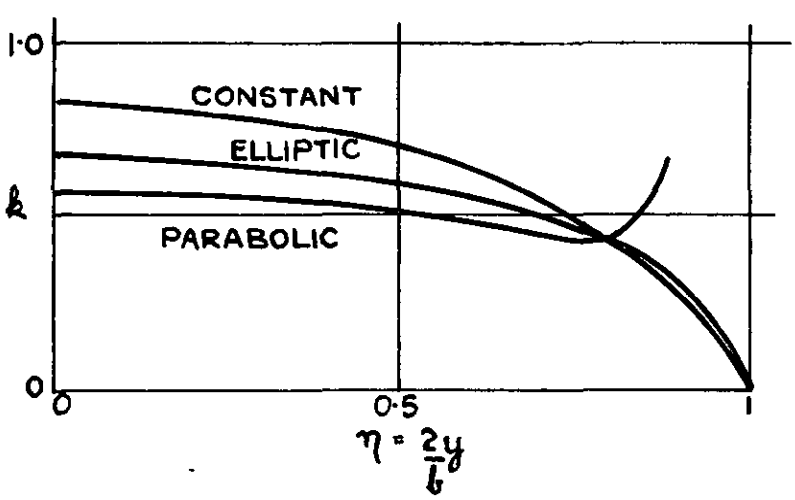

INFLUENCE OF CIRCULATION DISTRIBUTION ON THE CAMBER CORRECTION FACTOR OF THE QUADRATIC AEROFOIL.

FIG. 20

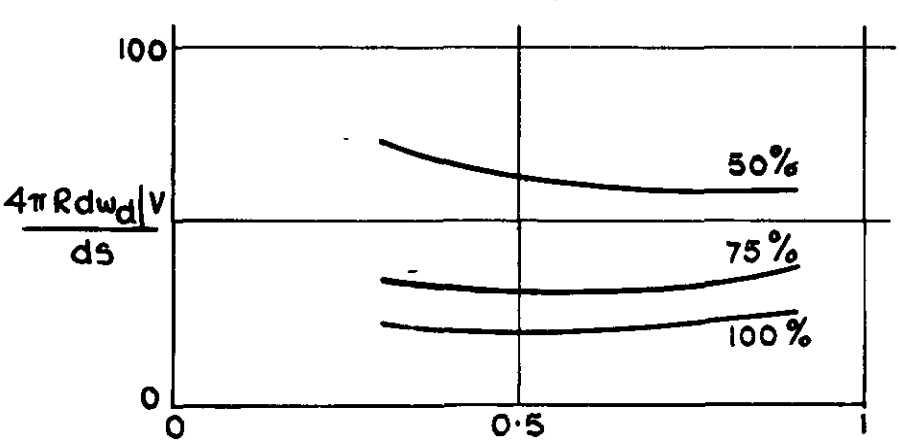

DOWNWASH DERIVATIVES FOR SHAPE-2 (FIG. 14)

$\Gamma = \frac{K x^2}{x^2 + \lambda^2}$

$\lambda_1 = 0{\cdot}2$

FIG. 21

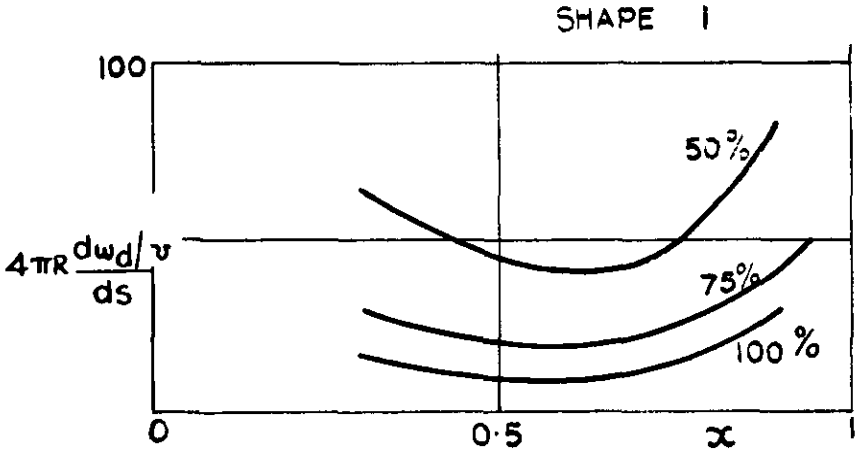

DOWNWASH DERIVATIVES FOR SHAPE 1 (FIG 13)

$\Gamma = \frac{K x^2}{x^2 + \lambda^2}$

$\lambda_1 = 0{\cdot}2$

FIG. 22

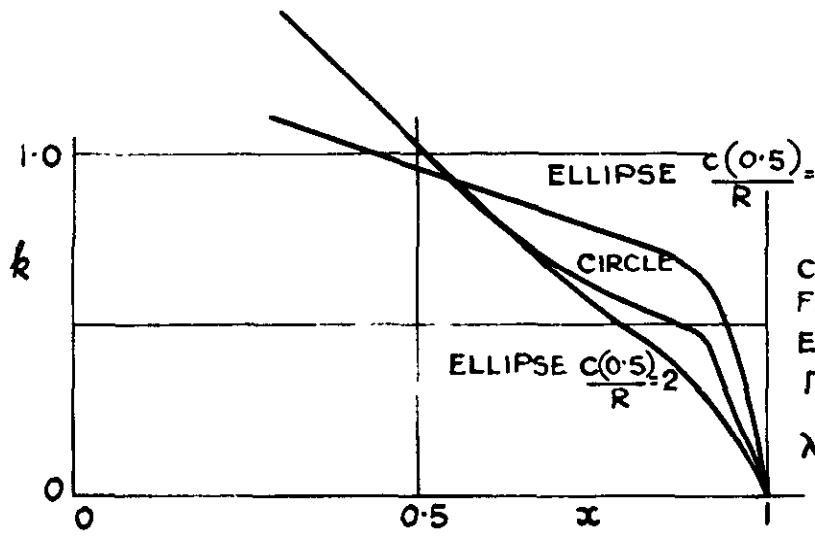

CAMBER CORRECTION FACTOR FOR ELLIPTICAL WINGS.

$\Gamma = \frac{K x^2}{x^2 + \lambda^2}$

$\lambda_i = 0{\cdot}2$

FIG. 23

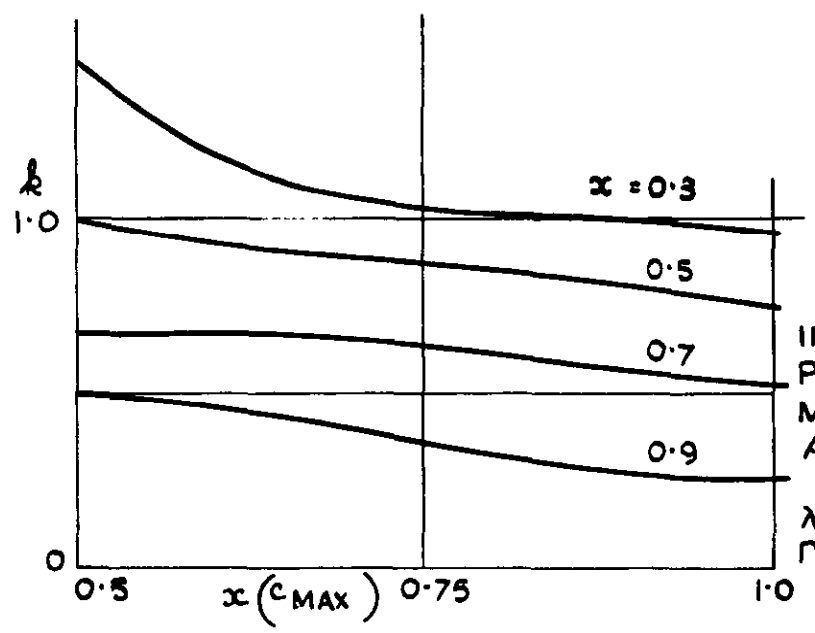

INFLUENCE OF POSITION OF MAXIMUM WIDTH

$A = \frac{R^2 \pi}{4}$

$\lambda_1 = 0{\cdot}2$

$\Gamma = \Gamma_{opt}$

FIG. 24

A.R.L | R3 | G | HV | 7 | 1

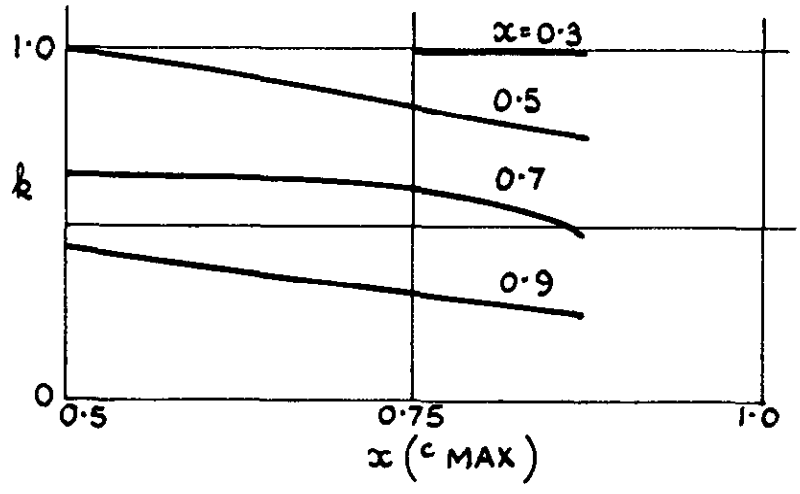

INFLUENCE OF POSITION OF MAXIMUM WIDTH
$A = 1{\cdot}25 \frac{R^2\pi}{4}$
$\lambda_1 = 0{\cdot}2$
$\Gamma = \Gamma opt$

FIG. 25

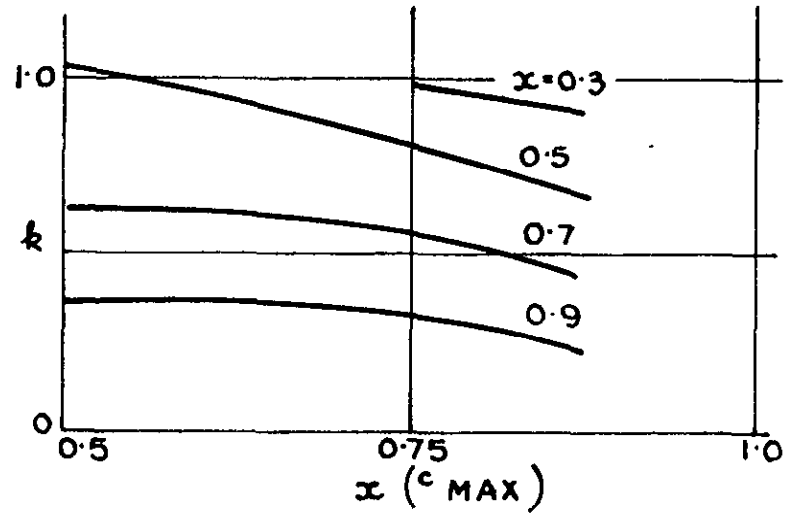

INFLUENCE OF POSITION OF MAXIMUM WIDTH
$A = 1{\cdot}5 \frac{R^2\pi}{4}$
$\lambda_1 = 0{\cdot}2$
$\Gamma = \Gamma opt$

FIG. 26

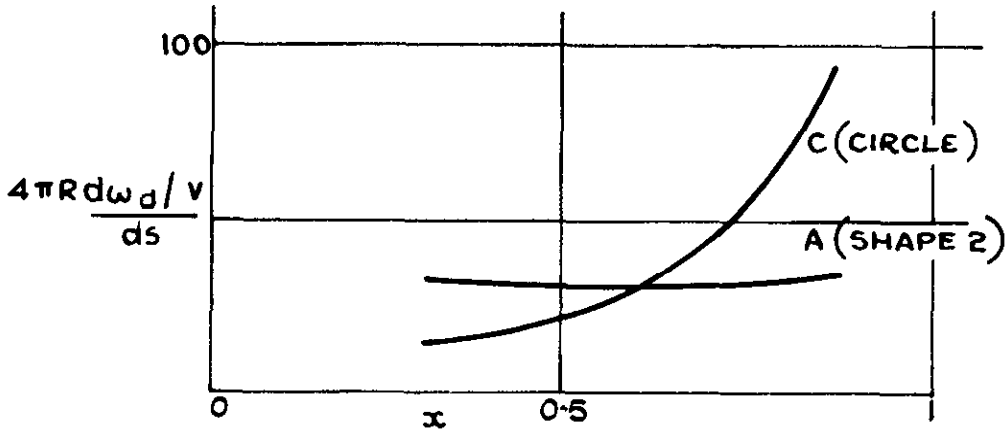

DOWNWASH DERIVATIVE FOR DIFFERENT SHAPES OF PROPELLER BLADES HAVING THE SAME WIDTH AT $x = 0{\cdot}5$.
$\Gamma = \Gamma opt = \frac{K x^2}{x^3 + \lambda}$

FIG 27

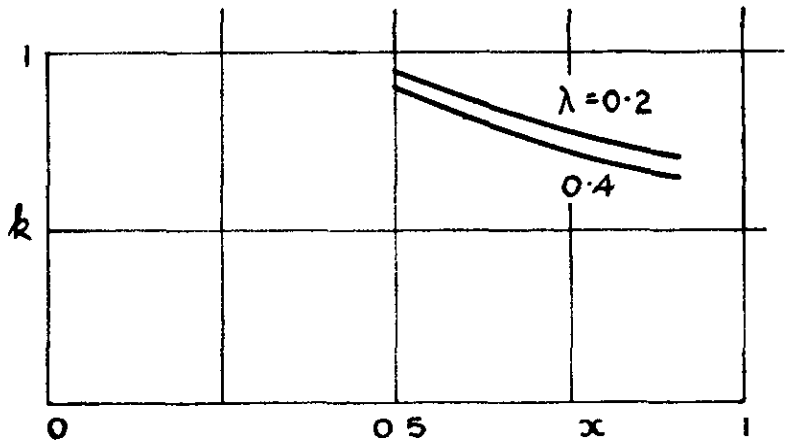

CAMBER CORRECTION FACTOR FOR THE ELLIPTIC PROPELLER BLADE $\frac{c(0.5)}{R}=\frac{1}{2}$

FIG. 28

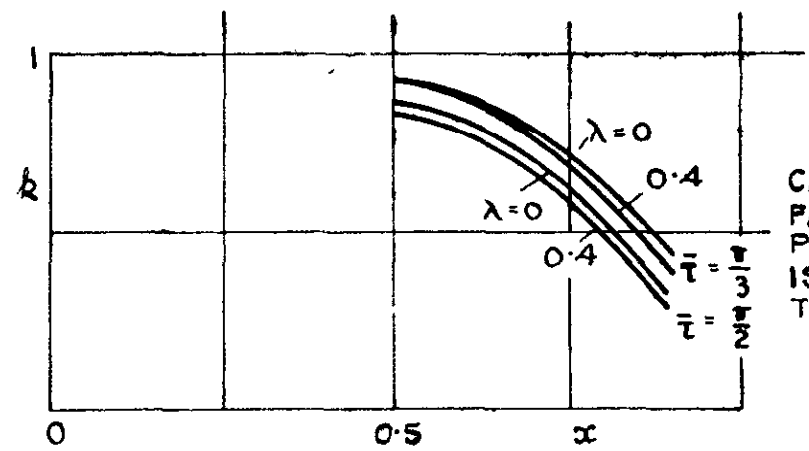

CAMBER CORRECTION FACTOR, THE PROJECTED SHAPE IS A SECTOR OF THE CIRCLE.

Γ = const

FIG. 29

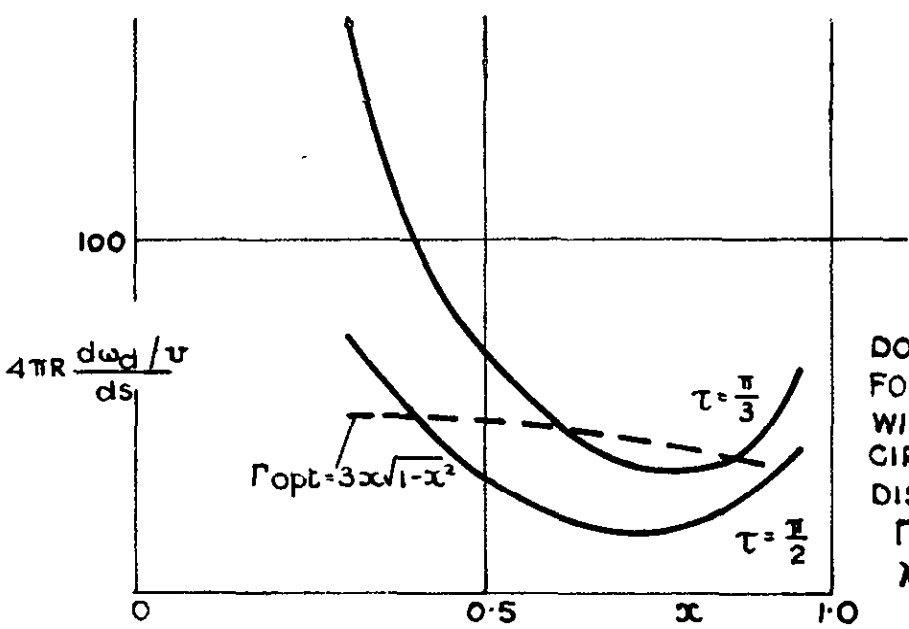

DOWNWASH DERIVATIVE FOR THE SECTOR BLADE WITH VARIOUS CIRCULATION DISTRIBUTIONS.

Γ = const = 1

$\lambda = 0$

FIG. 30

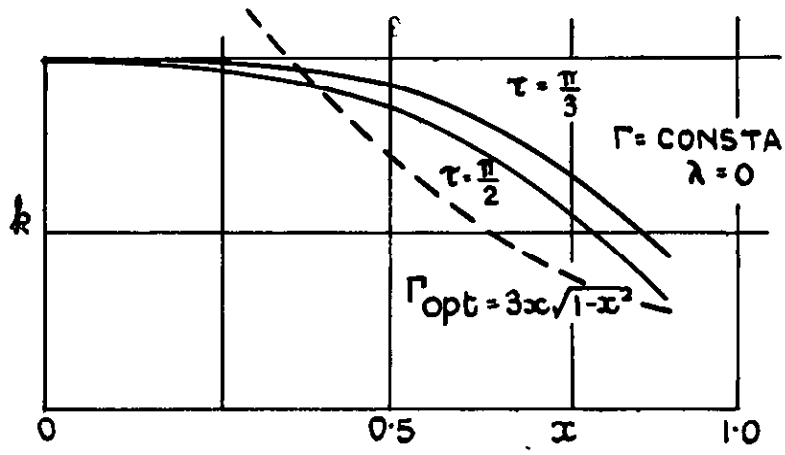

CAMBER CORRECTION FACTOR FOR THE SECTOR BLADE WITH VARIOUS CIRCULATION DISTRIBUTIONS.

FIG. 31

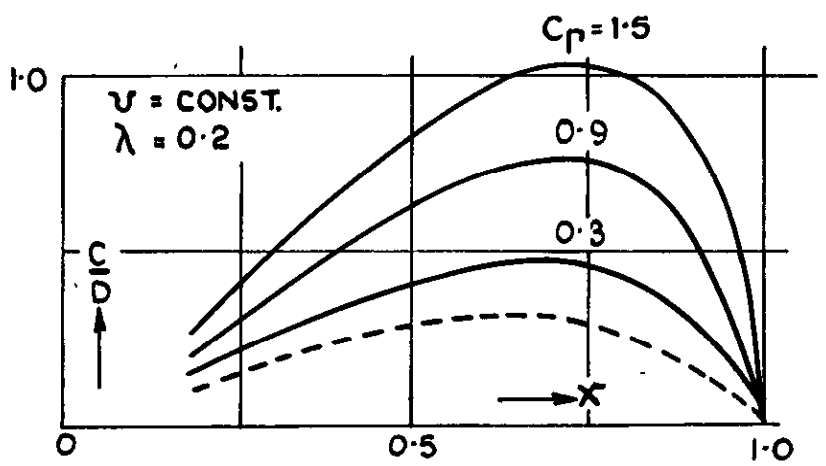

THE ADEQUATE BLADE FOR BEST DISTRIBUTION

FIG. 32 A

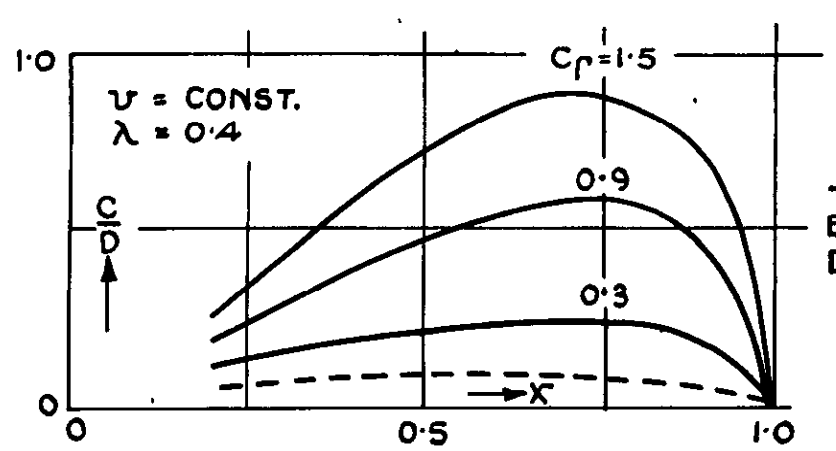

THE ADEQUATE BLADE FOR BEST DISTRIBUTION.

FIG. 32 B

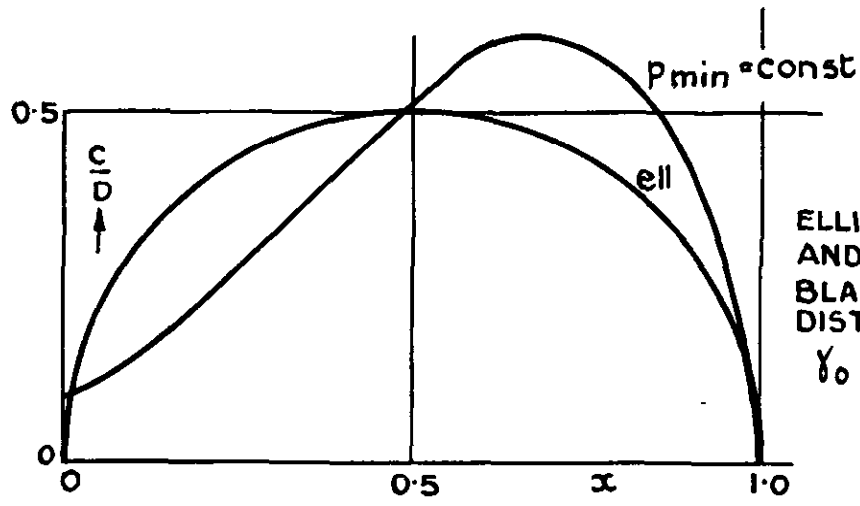

ELLIPTICAL BLADE AND ADEQUATE BLADE FOR BEST DISTRIBUTION.

$\gamma_0 = \frac{K x^2}{x^2 + \lambda^2}$

FIG. 34A

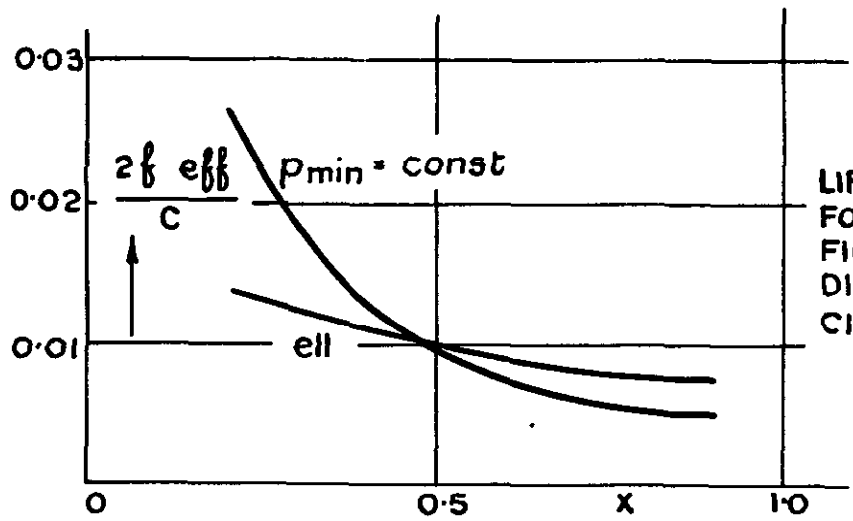

LIFT CO-EFFICIENTS FOR THE TWO BLADES FIG. 34A AND BEST DISTRIBUTION OF CIRCULATION.

FIG. 35A

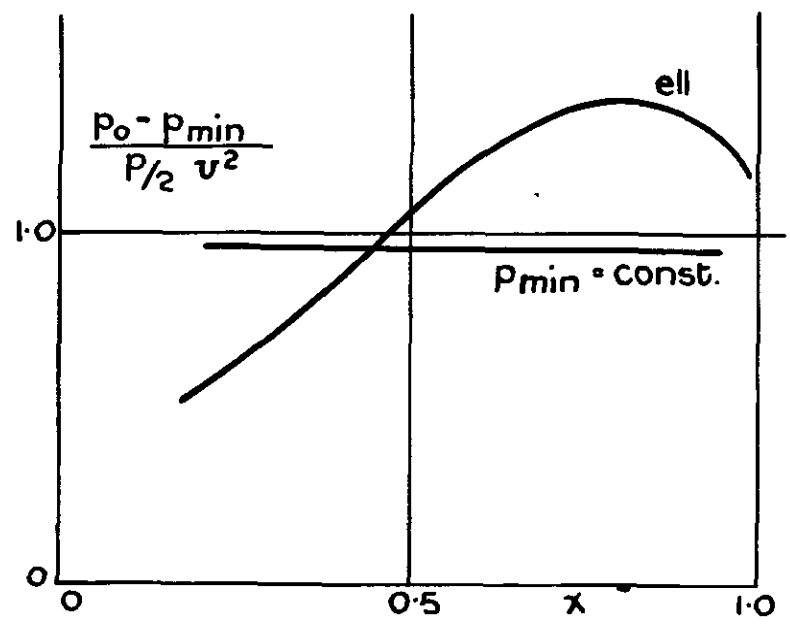

MINIMUM PRESSURE FOR THE TWO BLADES FIG. 34A AND BEST DISTRIBUTION OF CIRCULATION.

FIG. 36A

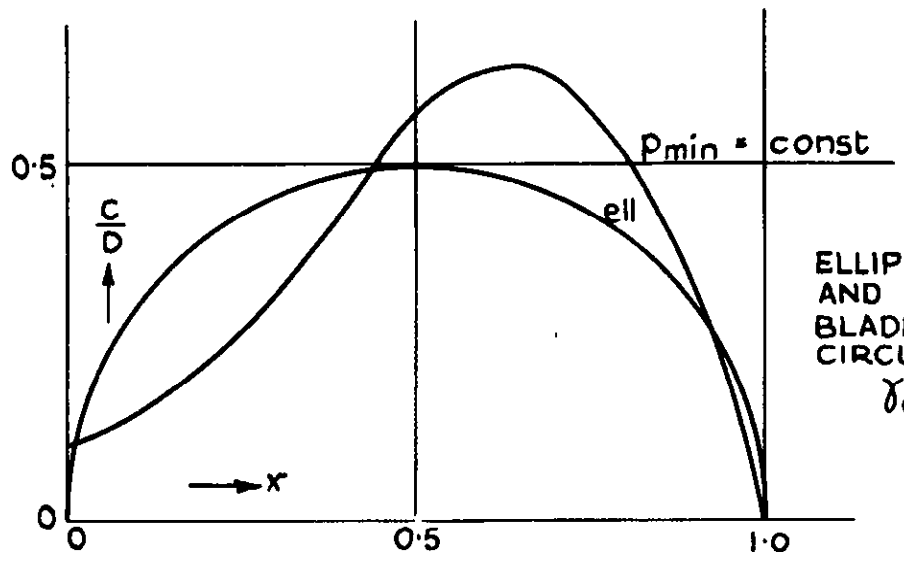

ELLIPTICAL BLADE AND ADEQUATE BLADE FOR CIRCULATION

$\gamma_0 = \sin x\pi$

FIG. 34 B

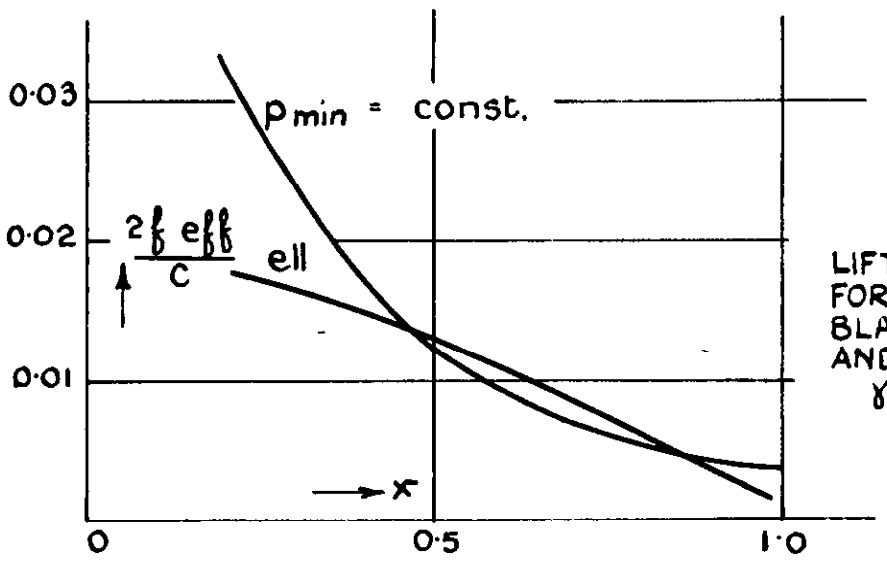

LIFT CO-EFFICIENTS FOR THE TWO BLADES FIG. 34 B AND

$\gamma_0 = \sin x\pi$

FIG. 35 B

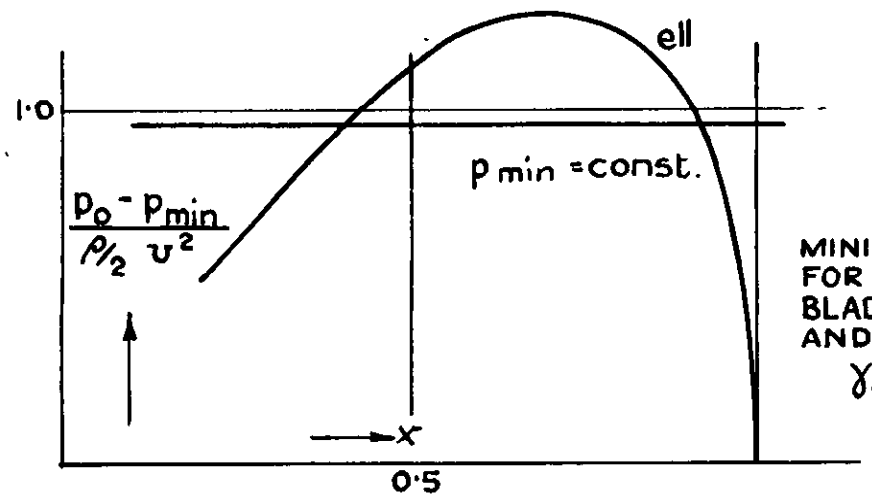

MINIMUM PRESSURE FOR THE TWO BLADES FIG. 34 B AND

$\gamma_0 = \sin x\pi$

FIG. 36 B

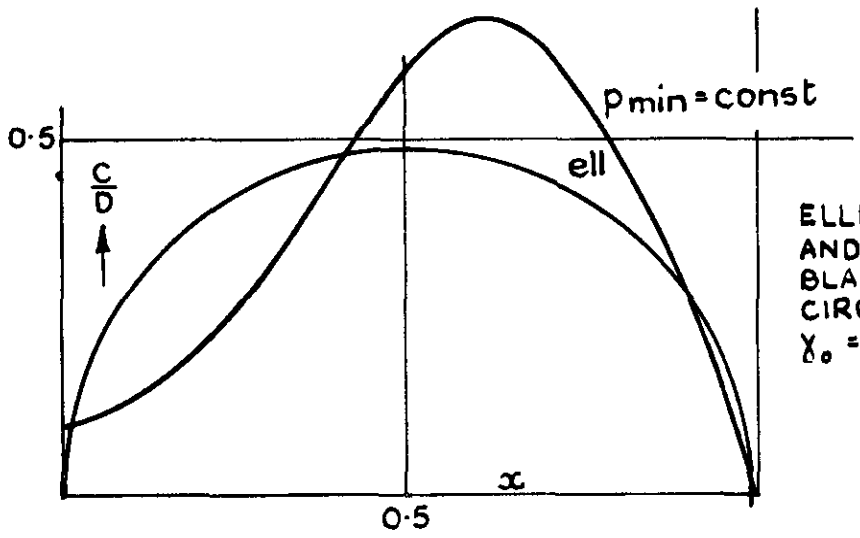

ELLIPTICAL BLADE AND ADEQUATE BLADE FOR CIRCULATION
$\gamma_0 = 1 + \sin\left(4x-1\right)\frac{\pi}{2}$

FIG. 34 C

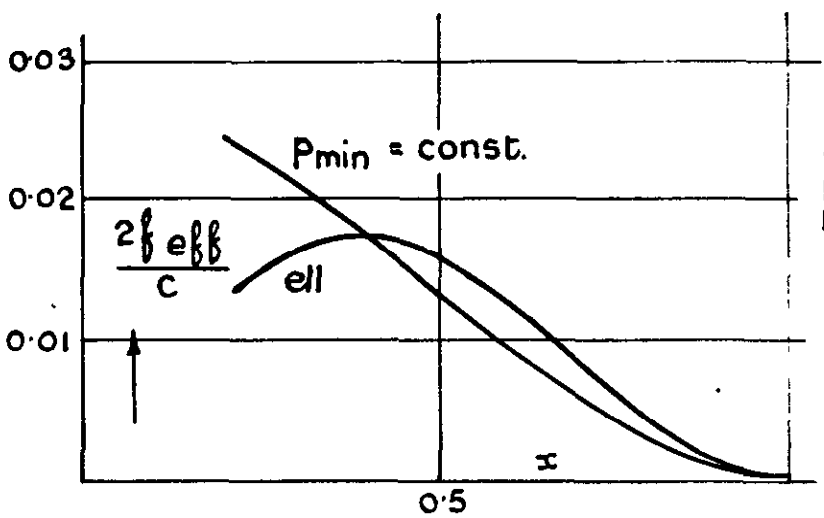

LIFT CO-EFFICIENTS FOR THE TWO BLADES FIG. 34C AND
$\gamma_0 = 1 + \sin\left(4x-1\right)\frac{\pi}{2}$

FIG. 35C

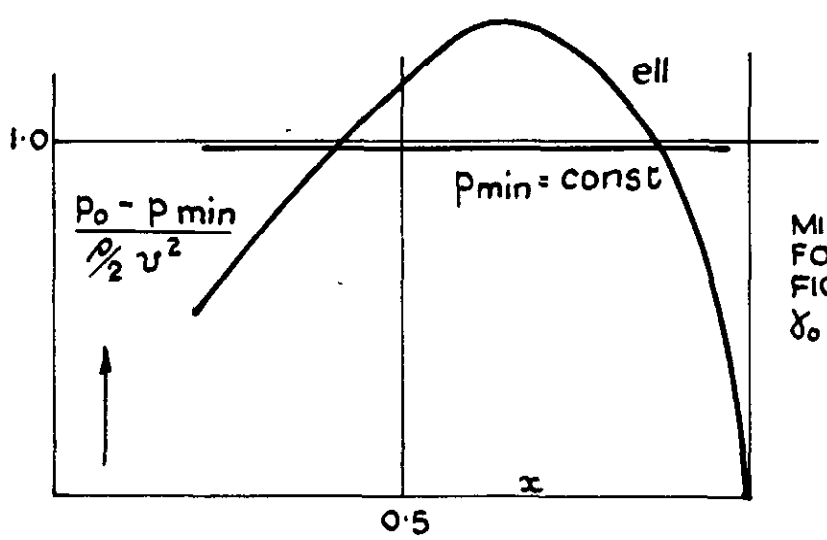

MINIMUM PRESSURE FOR THE TWO BLADES FIG. 34 C AND
$\gamma_0 = 1 + \sin\left(4x-1\right)\frac{\pi}{2}$

FIG. 36 C

A.R.L / R3 / G / HY / 7 / 1

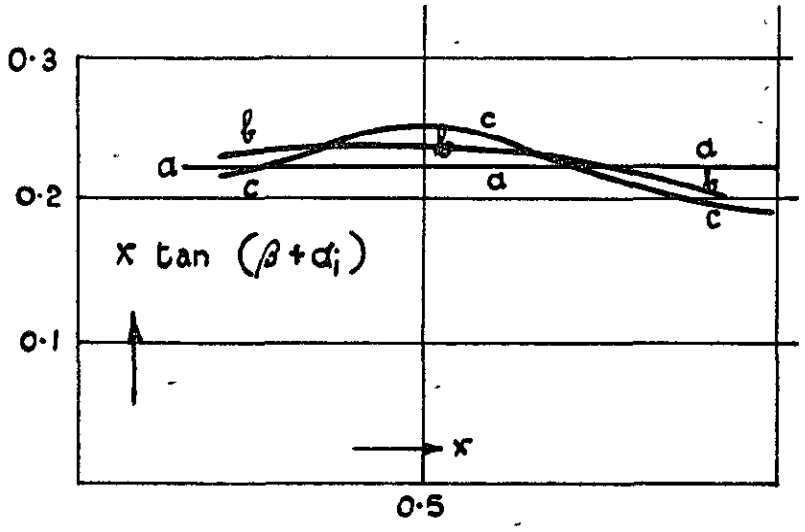

THE TWIST OF THE BLADE TO MAINTAIN SHOCK FREE ENTRY EVEN FOR THE CIRCULATION DISTRIBUTION
(b) $\gamma_0 = \sin x\pi$
(c) $\gamma_0 = 1+\sin(4x-1)\frac{\pi}{2}$

FIG. 37

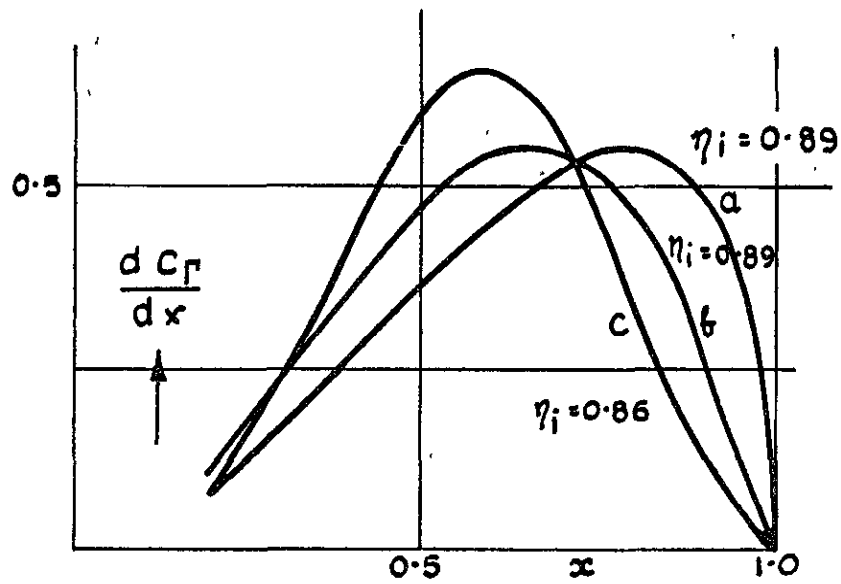

THRUST DISTRIBUTION FOR THE CIRCULATION DISTRIBUTION
(a) $\gamma_0 = \frac{kx^2}{x^2+\lambda^2}$
(b) $\gamma_0 = \sin x\pi$
(c) $\gamma_0 = 1+\sin(4x-1)\frac{\pi}{2}$

FIG. 38

A.R.L. / R3 / G / HY / 7 / 1

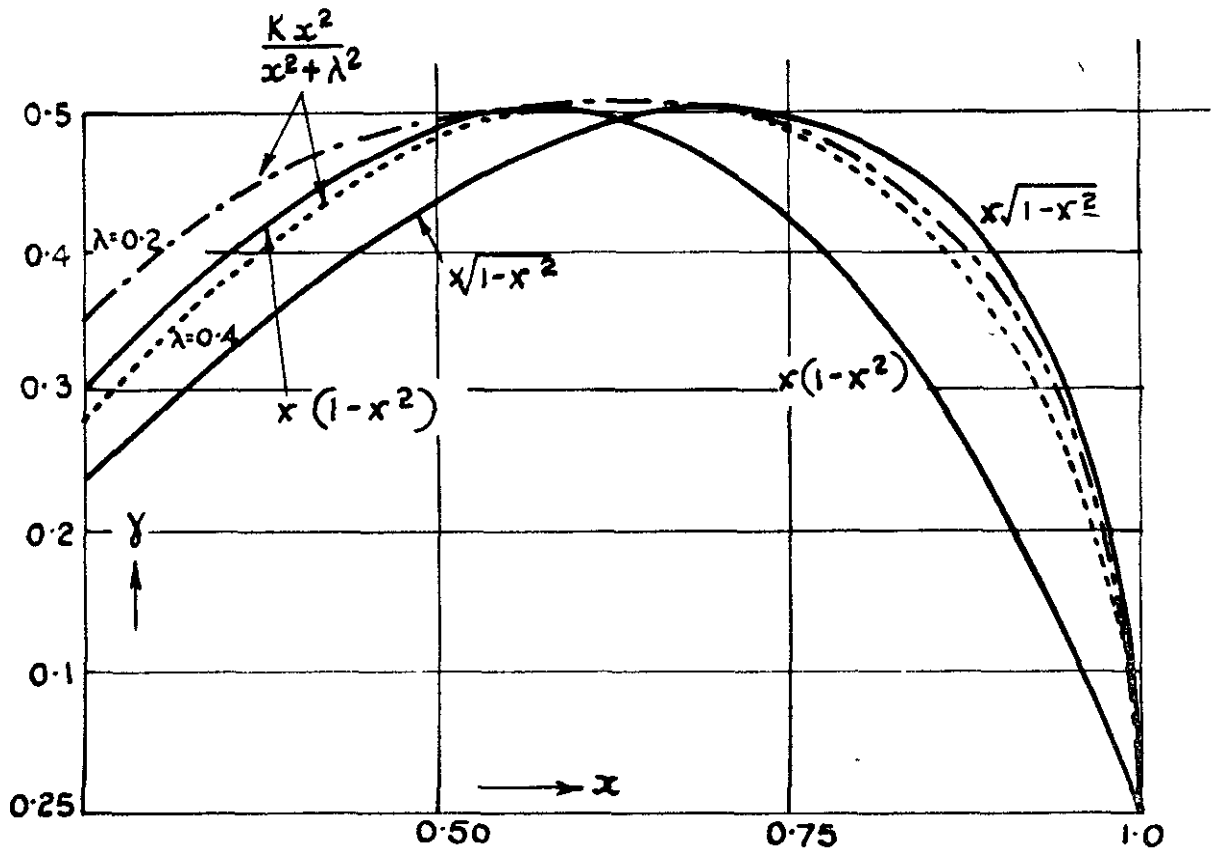

BEST DISTRIBUTION, LOCK'S APPROXIMATION AND THE PROPOSED CIRCULATION DISTRIBUTION.
$x(1-x^2)$

FIG. 39

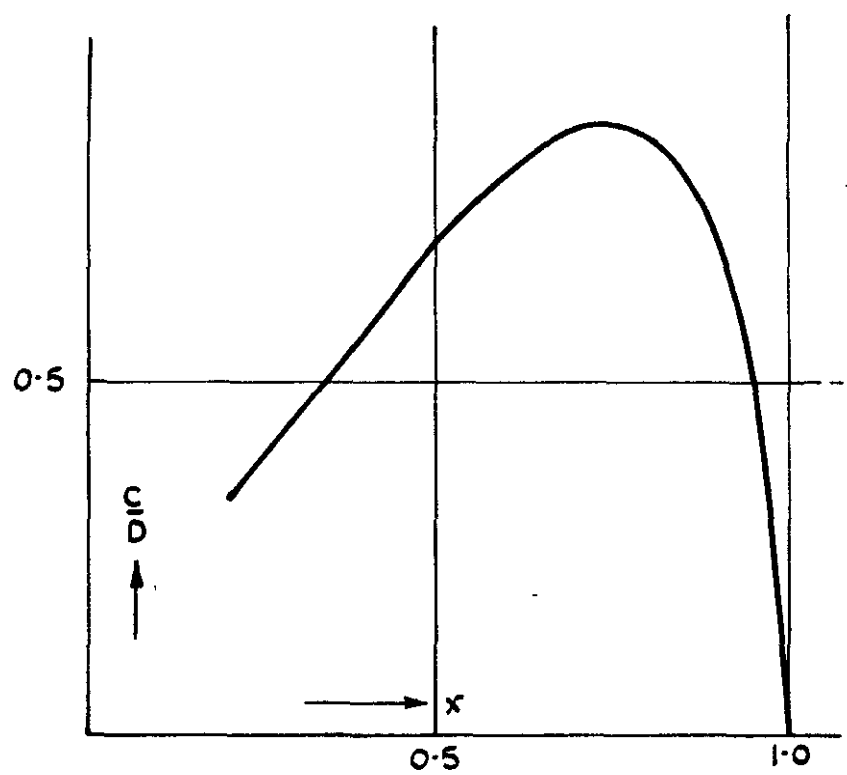

BLADE SHAPE FOR THE EXAMPLE.

FIG. 40

A.R.L / R3 / G / HY / 7 / 1

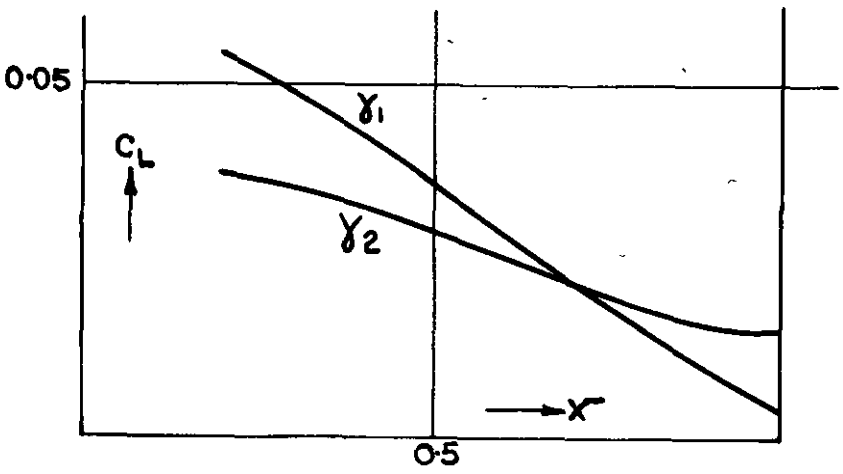

LIFT DISTRIBUTION FOR LOCK'S CIRCULATION γ_2 AND THE SUGGESTED CIRCULATION γ_1.

FIG. 41

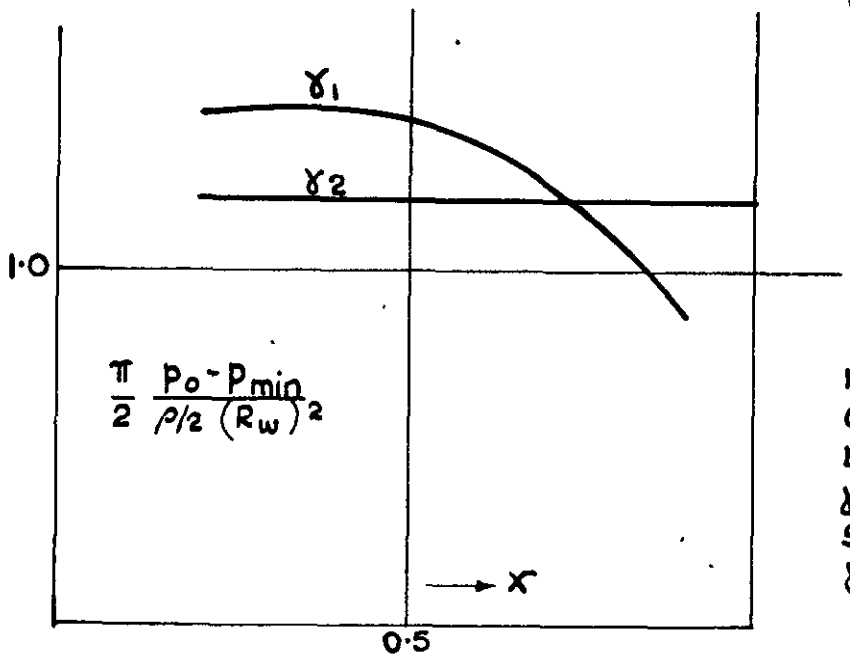

MINIMUM PRESSURE OVER RADIUS FOR LOCK'S CIRCULATION γ_2 AND THE SUGGESTED CIRCULATION γ_1

FIG. 42

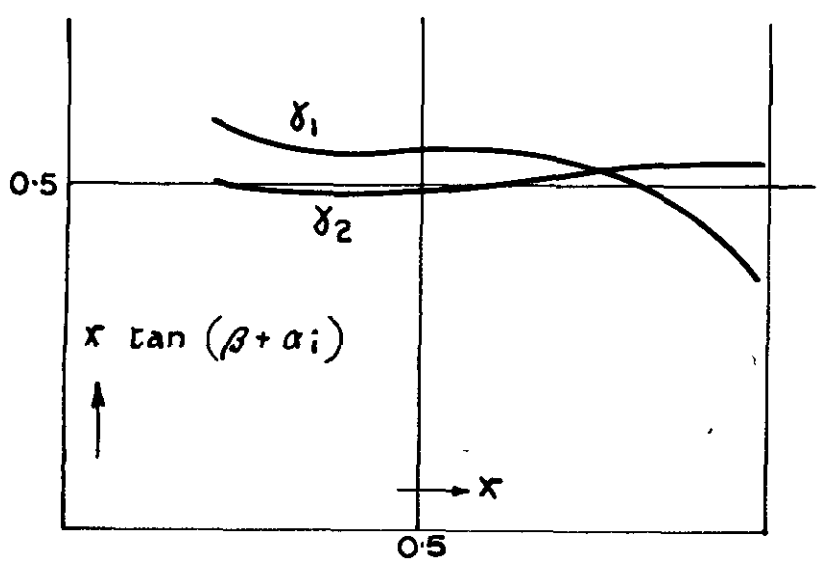

THE TWIST OF THE BLADE FOR LOCK'S CIRCULATION γ_2 AND THE SUGGESTED CIRCULATION γ_1

FIG. 43

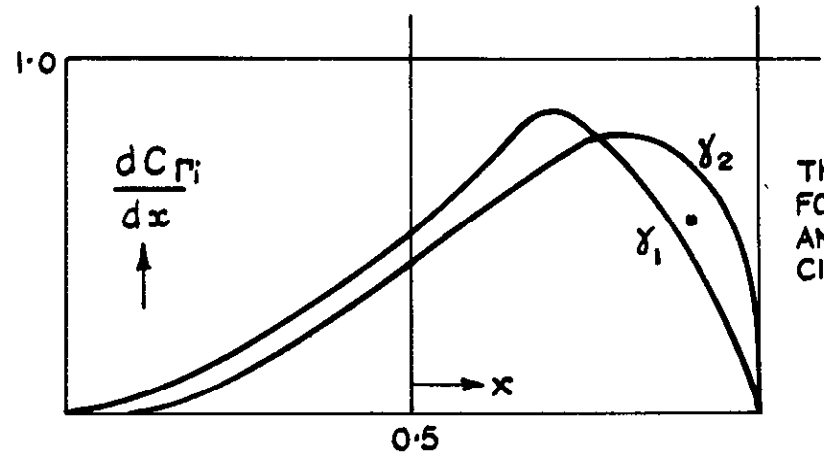

THRUST DISTRIBUTION FOR LOCK'S CIRCULATION AND THE SUGGESTED CIRCULATION γ_1

FIG. 44

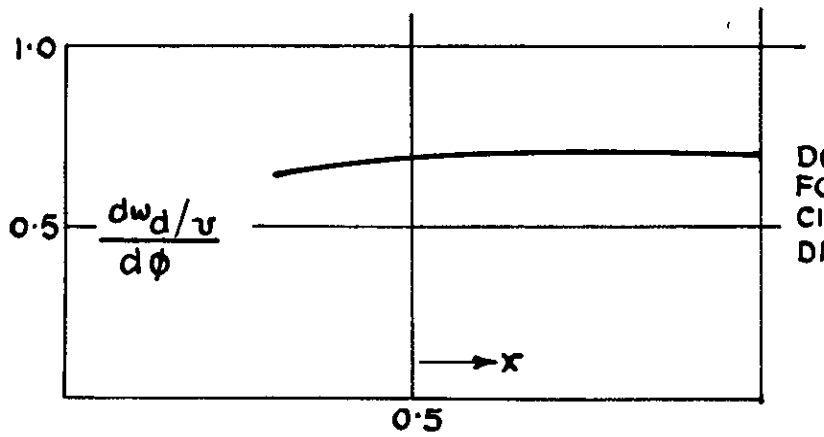

DOWNWASH DERIVATIVE FOR THE SUGGESTED CIRCULATION DISTRIBUTION.

FIG. 45

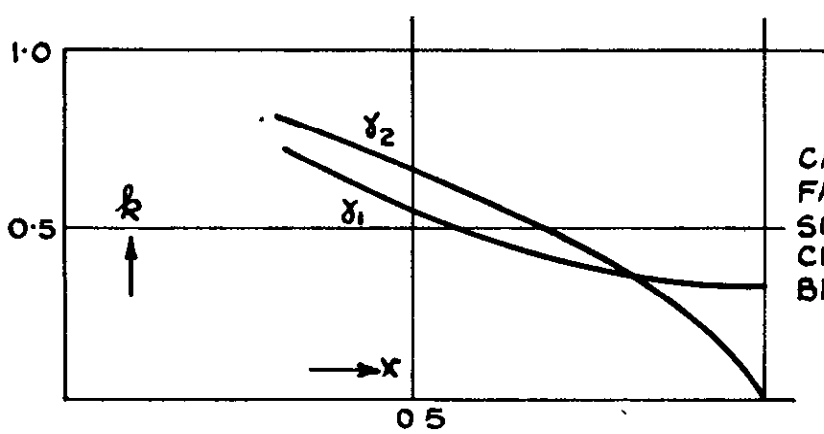

CAMBER CORRECTION FACTOR FOR THE SUGGESTED CIRCULATION γ_1 AND BEST DISTRIBUTION γ_2

FIG. 46

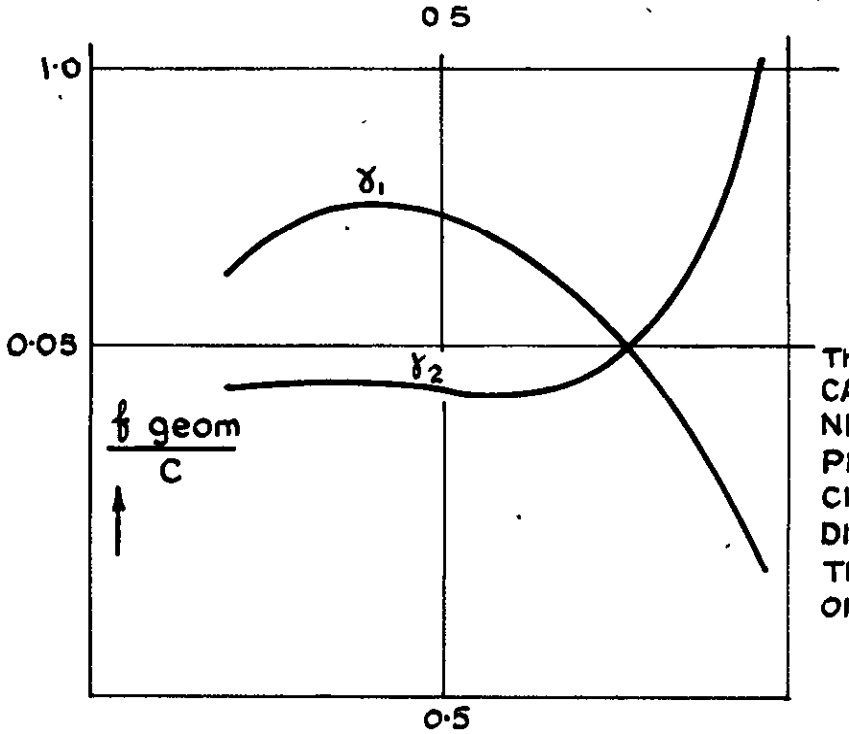

THE GEOMETRICAL CAMBER RATIOS NECESSARY TO PRODUCE LOCK'S CIRCULATION DISTRIBUTION γ_2 AND THE SUGGESTED ONE (γ_1).

FIG. 47

A.R.L/R3/G/HY/7/1

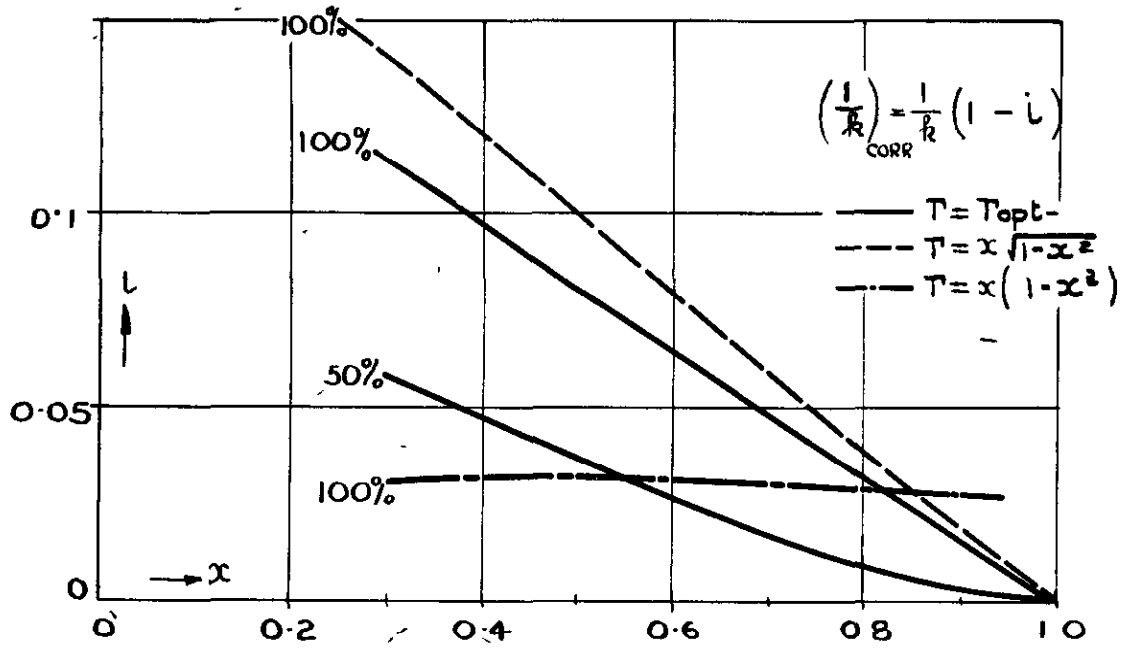

CORRECTION GIVING THE INFLUENCE OF THE SECOND AND THIRD BLADE ON THE CAMBER CORRECTION FACTOR k

BLADE SHAPE AS FIG. 40 [REF 1] CALLED 100% AND FOR A SIMILAR BLADE OF HALF THE WIDTH CALLED 50%

FIG. 48

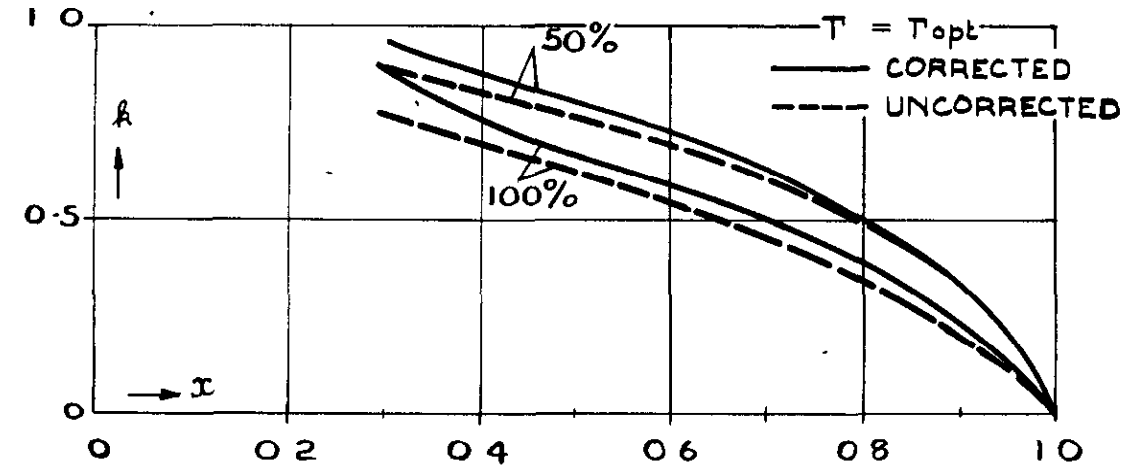

CAMBER FACTOR FOR BEST DISTRIBUTION OVER BLADE SHAPE FIG. 40 $\lambda = 0.4$

FIG. 49

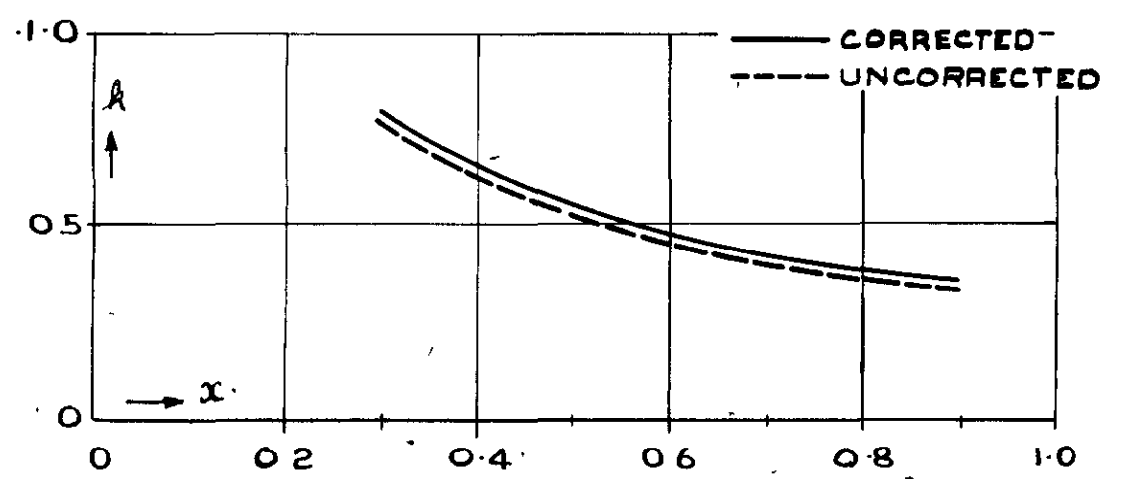

CAMBER FACTOR FOR THE DISTRIBUTION $T = x(1-x^2)$ OVER BLADE SHAPE FIG. 40 $\lambda = 0.4$

A.R.L. /R4/G/HY/7/1

FIG. 50

Crown Copyright Reserved

PRINTED AND PUBLISHED BY HER MAJESTY'S STATIONERY OFFICE

To be purchased from
York House, Kingsway, LONDON, W C 2 — 423 Oxford Street, LONDON, W 1
P O Box 569, LONDON, S E 1
13a Castle Street, EDINBURGH, 2 — 109 St Mary Street, CARDIFF
39 King Street, MANCHESTER, 2 — Tower Lane, BRISTOL, 1
2 Edmund Street, BIRMINGHAM, 3 — 80 Chichester Street, BELFAST
or from any Bookseller

1955

Price 6s 0d net

PRINTED IN GREAT BRITAIN